Title

Modeling and Optimization of Seawater Intrusion Barriers in Southern California Coastal Plain

Authors

Yeh, William W-G.
Bray, Ben

Publication Date

2006-04-01

Modeling and Optimization of Seawater Intrusion Barriers in Southern California Coastal Plain

William W-G. Yeh, Principal Investigator
Distinguished Professor and Chair
Department of Civil and Environmental Engineering
University of California, Los Angeles, CA 90095-1593
williamy@seas.ucla.edu

Ben Bray, Graduate Student
Department of Civil and Environmental Engineering
University of California, Los Angeles, CA 90095-1593
bbray@ucla.edu

UC Water Resources Center
Technical Completion Report Project
No. W-983
April, 2006

ABSTRACT

A five-layered confined-unconfined flow and transport models are developed and calibrated for the Alamitos seawater intrusion barrier in Southern California. The conceptual model is based on the geological structure of the coastal aquifer system, and the key parameters in the flow and transport models are calibrated using field measurements of hydraulic conductivity as well as head and concentration observations. Because of the abundance of point measurements of hydraulic conductivity, the heterogeneous and random hydraulic conductivity field for each of the five aquifers is estimated by the proposed geostatiscal method of natural-neighbor-kriging (NNK). The longitudinal and transverse dispersivities in the transport model are estimated by an inverse procedure that minimizes the least-squares error for concentration (LSE-CON). The minimum LSE-CON is achieved near 50 ft (15.2 m) and 5 ft (1.52 m) for the longitudinal and transverse dispersivities, respectively. The calibrated simulation model is linked with two optimization models to investigate alternatives for enhancing seawater intrusion barrier operations for the Alamitos Barrier Project in Los Angeles. Two types of management problems are analyzed the optimal scheduling problem (OSP) and the optimal well location problem (OWLP). The objective of the OSP is to minimize the total injected water subject to constraints on the state variables: hydraulic head and chloride concentration at target locations. Two OSP formulations are considered, a pure hydraulic gradient formulation, and a combined hydraulic and transport formulation. Optimization results suggest that algorithm performance is best when the number of decision variables can be limited to approximately ten wells. Next, a genetic algorithm is linked with the calibrated simulation model to determine the locations of new injection wells that maximize the marginal increase in head targets along the barrier. Parallel processing is also employed to improve algorithm efficiency.

INTRODUCTION

As population has grown in the Los Angeles County (LAC) throughout the 19th and 20th centuries and into the current decade, local groundwater has been a crucial resource to the numerous cities of Southern California. Currently, as much as 40% of the annual water supply in Southern California is derived from groundwater pumping. From about the 1940s through the 1950s, concern began to mount as monitoring data revealed rising chloride levels in wells close to the Pacific Coast (Callison *et al.*, 1991). To mitigate the growing threat of seawater intrusion from prolonged development and in some cases over-drafting of local aquifers, commencing in 1959 seawater barrier projects were implemented in LAC (Water Replenishment District of Southern California, 2004). These hydraulic barriers raise freshwater water head, creating a hydraulic gradient that prevents seawater from advancing inland and protects freshwater pumping wells in the coastal groundwater basins. As stated by Reichard and Johnson (2005) in their recent regional study of the Los Angeles County Basin, "[a] continuing water-management challenge, however, is to improve the effectiveness of seawater intrusion control."

The Los Angeles County Department of Public Works (LACDPW) currently operates three seawater barrier projects: the West Coast Basin, the Dominguez Gap, and the Alamitos Barrier Projects. In particular, the Alamitos Barrier Project (ABP) operates under the direction and approval of a joint committee representing the interests of both the Los Angeles County Flood Control District and the Orange County Water District. This study focuses on the model development and calibration of the Alamitos seawater intrusion barrier associated with the ABP.

This study addresses the urgent need to develop simulation-optimization models that can be used as tools in formulating and adapting management strategies to improve barrier operation. First a conceptual model of the Alamitos seawater intrusion barrier associated with the ABP is developed and calibrated. Then two important management scenarios are investigated by combining simulation and optimization models. In the first scenario, optimal injection policies that minimize the amount of injected water, while maintaining head and concentration targets, are identified for the existing barrier configuration. In the second scenario, optimal locations for new injection wells are identified that result in the greatest improvement in the hydraulic gradient along the barrier alignment.

While this study focuses solely on the ABP study site, the simulation-optimization tools and management approaches presented could be easily adapted to the other barriers operating in the area. In contrast with this study, Reichard and Johnson (2005) use simulation-optimization modeling to examine alternatives for reducing future seawater intrusion on a regional basis for all of Los Angeles County. Reichard and Johnson (2005) simulated the regional groundwater flow in Los Angeles County with MODFLOW (Harbaugh and McDonald, 1996), producing the response matrix subsequently incorporated as linear constraints in the optimization formulation and solved with LINDO (Schrage, 1993). The elements of the response matrix relate the state variable, in their case predicted head, to the injection policy where the head is maintained at or near a target level while the cost of purchased water is minimized.

Study Site Description

The ABP study area, shown in Figure 1, includes parts of the city of Long Beach in Los Angeles County, and the cities of Los Alamitos and Seal Beach of Orange County. The ABP was initiated to protect the groundwater supplies of the Central Basin of Los Angeles County and the East Coastal Plain of Orange County from seawater intrusion through the Alamitos Gap. The ABP, and all other barriers in Los Angeles County, are operated under the direction and approval of a joint committee representing the Los Angeles County Flood Control District and the Orange County Water District (Callison *et al.*, 1991). The County of Los Angeles Department of Public Works carries out daily operations and maintenance of the barriers, and the Water Replenishment District of Southern California is responsible for maintaining the water supply to each barrier. Roughly 4,600 acre-feet ($7.931*10^6$ m^3) of imported water are injected annually through 43 injection wells along the barrier. The ABP injection wells operate continuously with injection rates ranging from 0.05 to 1.5 cfs (0.00142 to 0.04248 cms). Extemporaneous adjustments to injection rates of the various barrier wells are currently made based on a range of factors including water level elevations and chloride concentrations in the observation wells, local groundwater conditions, and individual injection well performance.

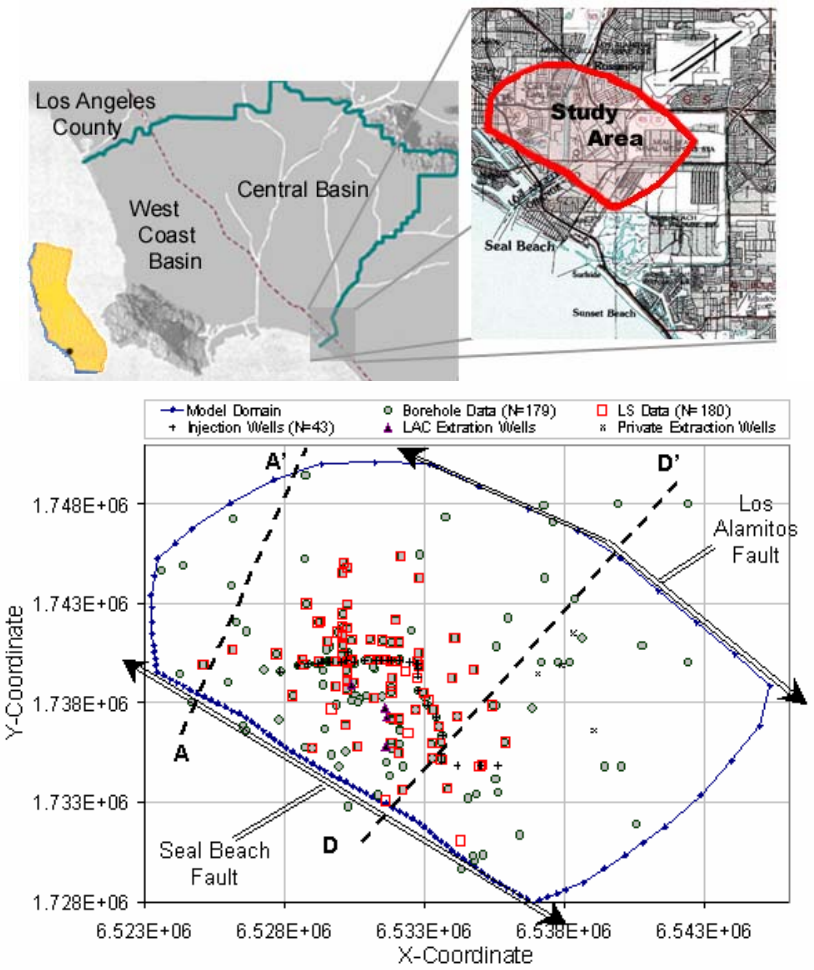

Figure 1: Alamitos Study Site Area Map, Plan View of Model Domain, and Observation Well Networks for Model Building and Calibration.

Geological Description

The Alamitos seawater intrusion barrier is located at the southern coastal boundary of Los Angeles County. The model domain in relation to local faults and the distribution of two monitoring well networks will be described later in greater detail. Like most of the Los Angeles Basin, the Alamitos site is comprised of alternating layers of conductive alluvium capped by less conductive mud and clay layers. The shape and composition of these layers is further complicated by the action of local faults and rivers. With respect to the Alamitos study site, two local faults run parallel to the coast and delineate the northeast and southwest model boundaries, these are the Seal Beach and Los Alamitos Faults. Two cross sections in Figure 2a and 2b demonstrate the local geologic complexity and also delineate the local faults. The injection well barrier is aligned in a zigzag pattern between two Upper Pliestocene Quarternery formations (Callison *et al.*, 1991): Bixby Hill to the north, and Landing Hill to the south.

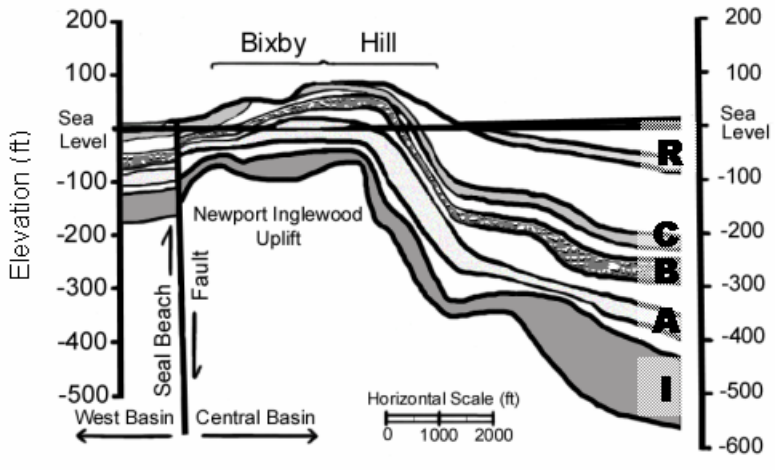

(a) Cross-Section A-A'

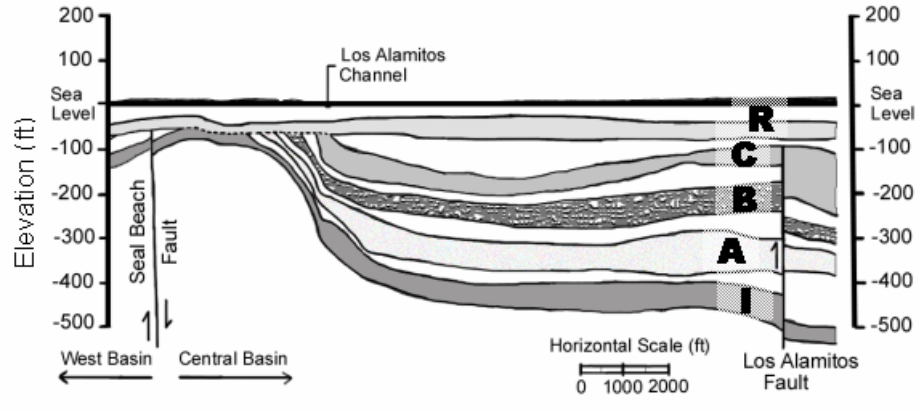

(b) Cross-Section D-D'

Figure 2: Cross-Sections Through Alamitos Barrier Project Study Site Adapted from Callison *et al.* (1991). (a) Northern cross-section A-A' through Bixby Hill; (b) Southern cross-section D-D'.

Callison *et al.* (1991) summarized the geology of the ABP area, providing much of the necessary data required to build the conceptual model of the study site. The following list summarizes a few key attributes of the local geology.

- The ABP area consists of five representative aquifers and four aquitards between them. The Recent Aquifer, the shallowest unconfined aquifer and abbreviated R, is a depositional feature of alluvial deposits from the San Gabriel and other local rivers, while the mid layer Lynwood formations (*i.e.* C, B, A, and I aquifers in order of increasing depth) are a sequence of depositional features from sea level fluctuations long ago. The C, B, A, and I aquifers are essentially confined although some regions of these aquifers are hydraulically connected to the unconfined R Aquifer in mergent zones. The deepest aquifer that receives injected water, the I Aquifer, is approximately 450 ft below sea level.

- Local geologic complexity is heightened by indigenous channels, like the San Gabriel River, because of their persistent presence during the developmental stages of the various geomorphic layers.

- A and I Aquifers within the Lynwood formation are the most important in terms of controlling seawater migration inland, particularly because these layers are relatively conductive layers composed of fine sands and gravels.

- The local faults (Los Alamitos and Seal Beach) offset the aquifers and aquitards, essentially disconnecting them from adjacent basins (see cross sections in Figures 2a and 2b). Furthermore, because of vertical and lateral movements, particularly in the more active Seal Beach Fault, these features effectively act as a barrier to seawater encroachment.

- The primary mechanism of seawater intrusion to deeper aquifers is vertically from the R aquifer following lateral intrusion from the ocean. Seawater migrates into the R aquifer horizontally then travels to deeper layers primarily through mergent areas where aquitards evanesce, causing upper and lower aquifers to merge together. Once in the lower layers, seawater moves inland towards the Los Alamitos Fault.

Currently, the ABP consists of 43 injection wells and four extraction wells operating between the barrier and the coastline. The extraction wells are intended to enhance the hydraulic gradient around the barrier while intercepting some of the advancing seawater. Four additional private production wells also are operating inland from the barrier within the model domain. Extensive historical records of injection and extraction rates for all wells under the purview of LACDPW are available while private production data are limited.

OBJECTIVES

The first objective is to build and calibrate a conceptual model of the Alamitos seawater intrusion barrier associated with the ABP. Following conceptual model development, a two-phase calibration procedure is proposed for parameter estimation in which two different techniques are applied to calibrate a large-scale, density-dependent seawater intrusion model. In the first phase the dominant parameter for the flow model, the hydraulic conductivity field, is calibrated. The field is estimated for each element associated with a finite-element model in the flow domain by a modified kriging

technique called natural-neighbor-kriging (NNK). In the second calibration phase, the optimal transport parameter values are determined by an inverse procedure that minimizes the least-squares error. The dominant transport parameters are the longitudinal and transverse dispersivities, where the latter is constrained to be an order of magnitude less than the former. A measure of the model error, the least-squares error (LSE), is calculated over a reasonable range in the parameter values, and the optimal parameter values are those that minimize the LSE.

The second objective is to examine ways of improving the Alamitos barrier operation and effectiveness in mitigating seawater intrusion through the use of simulation-optimization modeling. To meet this objective two management problems are investigated for improving the efficiency of the Alamitos barrier: first to improve upon the operation of the existing barrier configuration, and second to identify the optimal locations for new injection wells. The scenarios presented in this study demonstrate how these simulation-optimization models can be used to improve barrier operations, and provide insight as to their performance.

Problem 1: Improving Existing Barrier Operations

In the first problem, the existing configuration of injection wells is optimized to quantify the minimum amount of water injected, such that specified head and concentration targets are maintained. The decision variables are the injection rates of existing wells under the purview of Los Angeles County Department of Public Works, and the state variables are head and concentration predicted by the calibrated groundwater simulation model. This optimization problem, henceforth referred to as the optimal scheduling problem (OSP), is effectively a nonlinear programming problem because head and concentration constraints are nonlinear functions of injection rates, and continuous since the injection rates are permitted to vary continuously between an operational minimum and maximum in each management period.

Problem 2: Identifying Optimal Candidate Sites for New Injection Wells

The second management scenario is to consider the optimal placement of new injection wells added to the existing barrier. The second management scenario, termed the optimal well location problem (OWLP), is solved by linking a genetic algorithm (GA) to the simulation model. In the GA each individual chromosome string defines a unique injection well configuration, which is fed to the simulation model to provide the quantitative benefit associated with the given configuration. In this case the benefit or fitness function is the marginal gain in the hydraulic gradient along the barrier alignment above the baseline scenario in which no new wells are added.

PROCEDURES

Seawater Intrusion Modeling Approaches

In terms of mitigating seawater (saltwater) intrusion, some researchers like Reichard and Johnson (2005) for example, have approached the problem indirectly, focusing only on maintaining pressure head above a designated level. In this case maintaining head along a barrier at or above mean sea level is intended to control future seawater intrusion and involves only the solution of the groundwater flow model. However, in dealing directly with both the transport of seawater and groundwater flow, two predominant approaches have been pursued – the sharp and disperse interface approaches – the former being a simplified case of the latter. Under the sharp interface approach, saltwater and freshwater are considered two immiscible fluids of constant density with a common interface where pressure continuity is maintained. The sharp interface approach was preferred in earlier studies because it is relatively easier to implement and does not require the coupling of flow and transport. Many variations of the sharp interface approach can be found in the literature (see for example Shamir and Dagan, 1971; Wilson and Sa da Costa, 1982; and Essaid, 1990). The fundamental disadvantage of the sharp interface approach is that only a rough approximation of the saltwater wedge location and evolution can be estimated.

Alternatively, the disperse interface approach more accurately accounts for the spatial and temporal variations in saltwater concentration and density within a coastal aquifer. The dissertation by Henry (1960) was one of the first to intensively compare sharp and disperse interface approaches. Henry developed a closed form analytic representation of the disperse interface model for a simple test case that eventually evolved into the widely known Henry's problem. Advances in computing apparently have led to a boom in the popularity of groundwater simulation models that implement the more general disperse interface approach (Simmons, 2005). A corresponding rise in the popularity of Henry's problem has established a benchmark for testing and validating these numerical models (Croucher and O'Sullivan, 1995).

In the context of groundwater modeling, the disperse interface approach is more commonly known as the density-dependent (DD) approach. DD models have been applied successfully in many hydrogeological contexts. Gupta and Bair (1997), for example, developed a regional DD model to study how density impacts vertical and horizontal fluxes as deep salt formations interact with the overlying aquifer formations. Schincariol and Schwartz (1990) studied the interaction of mixing and heterogeneity in DD flow while Frind (1982) investigated the long-term implications of applying DD models relative to other approaches. Koch and Zhang (1993) utilized a DD model in a different context, investigating the transport of contaminant plumes originating from a landfill source. While the use of DD models has increased in the last two decades, as Simmons (2005) argues, there are still plenty of opportunities for future research and development to improve upon them.

Conceptual Model Development

The southwest and northeast model boundaries are the Seal Beach and Los Alamitos Faults, respectively while the northwest and southeast boundaries are extended a few thousand feel away from the barrier to minimize boundary effects. The study area is approximately four and one quarter miles wide and close to 3 miles in between the two faults covering an area close to 11 square miles. Nine distinct geologic layers are represented in the model beginning with an unconfined aquifer containing areas of partial saturation (*e.g.* Bixby Hill) followed by a sequence of aquitards and aquifers (the layers are shown in Figure2a and 2b). Only layers directly affected by the injection wells are included with the exception of the upper unconfined R Aquifer.

The flow and transport models, respectively presented below, describe the functional variation in the hydraulic pressure field (h) and the constituent concentration (C) with respect to the three Cartesian coordinates (x, y, z) and time (t). Saltwater conventionally is treated as a conservative contaminant, a reasonable assumption since chloride adsorption, decay, and reaction effects are minimal, and therefore are not included in the transport model. The governing equations for flow and transport can be represented as follows (Lin *et al.*, 1997):

$$\frac{\rho}{\rho_0} F \frac{\partial h}{\partial t} = \nabla \bullet \left[\vec{K} \left(\nabla h + \frac{\rho}{\rho_0} \nabla \vec{z} \right) \right] + \frac{\rho^*}{\rho_0} q \tag{1}$$

$$\theta \frac{\partial C}{\partial t} + \vec{V}_D \bullet \nabla C - \nabla \bullet \left(\theta \vec{D} \bullet \nabla C \right) = - \left(\left(\alpha \rho_0 g \right) \frac{\partial h}{\partial t} \right) \theta C + m - \frac{\rho^*}{\rho} qC + \left(F \frac{\partial h}{\partial t} + \frac{\rho_0}{\rho} \vec{V}_D \bullet \nabla \left(\frac{\rho}{\rho_0} \right) - \frac{\partial \theta}{\partial t} \right) C \tag{2}$$

$$F = \left(\alpha \rho_0 g \right) \frac{\theta}{n} + \left(\beta \rho_0 g \right) \theta + n \frac{dS}{dh} \tag{3}$$

$$\vec{K} = \frac{\rho g}{\mu} \vec{k} \tag{4}$$

$$\theta \vec{D} = \alpha_T \left| \vec{V} \right| \delta + \left(\alpha_L - \alpha_T \right) \frac{\vec{V} \vec{V}}{\left| \vec{V} \right|} + a_m \theta \tau \delta \tag{5}$$

$$\vec{V}_D = -\vec{K} \bullet \left(\frac{\rho}{\rho_0} \nabla h + \nabla \vec{z} \right) \tag{6}$$

$$\frac{\rho}{\rho_0} = a_1 + a_2 C \tag{7}$$

Equation 1 is the conservation of mass equation where head h [L] is related to the fluid density ρ [ML^{-3}], the freshwater density ρ_0 = 1.9383 slug/ft^3, the injected fluid density ρ^* [ML^{-3}], the specific source or sink per element volume q [T^{-1}], and time t [t]. The divergence and gradient operators are represented with the respective notations $\nabla \cdot$ and ∇. The predominant coefficients in Equation 1, the specific storage F [L^{-1}], and

hydraulic conductivity tensor $\vec{K}$ [LT^{-1}], are calculated with Equations 3 and 4, respectively. In Equation 3, α is the coefficient of consolidation of the soil [LT^2M^{-1}], g is the gravitational acceleration constant (9.81m/sec^2), θ is the moisture content, n is porosity, β is the compressibility of the fluid [LT^2M^{-1}], and the last term describes the differential change in saturation, S, with head and is either empirically known or typically estimated using a standard van Genutchen model (Lin *et al.*, 1997). In Equation 4, μ [$ML^{-1}T^{-1}$] is the dynamic viscosity of water and $\vec{k}$ [L^2] is the intrinsic permeability tensor.

In the advection dispersion model in Equation 2, C [ML^{-3}] represents the constituent concentration, m is the external source or sink rate per medium volume [$ML^{-3}T^{-1}$], $\vec{V}_D$ [LT^{-1}] is the Darcy velocity computed with Equation 6, $\vec{D}$ [L^2T^{-1}] is the dispersion tensor, and all remaining variables have been defined previously. The third term in Equation 2, the gradient of the surface flux containing the transport parameter $\vec{D}$, is calculated from Equation 5 where α_L [L] is the longitudinal dispersivity, α_T [L] is the transverse dispersivity, δ is the Dirac delta function, $\vec{V}$ [LT^{-1}] is the fluid velocity and is proportional to $\vec{V}_D$, a_m [L^2T^{-1}] is the molecular diffusion coefficient, and τ is the tortuosity. The key transport parameters calibrated in phase two are α_L and α_T which influence the shape, extent, and degree of saltwater dispersion within the aquifer. The molecular diffusion a_m, and consequently the last term in Equation 5, are assumed to be negligible in practice.

Equation 7 describes a typical first-order relationship that links the variation in concentration to fluid density. For saltwater intrusion the parameter a_1 is equal to unity and dimensionless; but a_2 generally has dimensions equivalent to the inverse concentration [L^3M^{-1}], and therefore depends upon the constituent of interest. The parameter a_2 provides the essential link between the flow and transport equations in the density-dependent approach. Furthermore, the interdependence among the dependent variables, h, V, ρ, and C in Equations 1, 2, 4, 5, 6, and 7 complicates the numerical solution of the flow and transport models.

A number of boundary conditions were experimented with during the calibration process. However, to match head and concentration trends in observation wells, the Dirichlet condition is preferred and is the exclusive boundary condition applied in this study. The Dirichlet boundary conditions for the dependent variables are as follows.

$$h = h_d\left(x_b, y_b, z_b, t\right) \text{ on } B_d \tag{8}$$

$$C = C_d\left(x_b, y_b, z_b, t\right) \text{ on } B_d \tag{9}$$

In Equations 8 and 9, the subscript d delineates the Dirichlet condition, while the subscript b delineates the boundary coordinates that belong to the Dirichlet boundary node set B_d. Initial conditions simply are represented as the two dependent variables specified for all discretized coordinates in the problem domain or $h(x,y,z,0)$ and $C(x,y,z,0)$. The boundary and initial conditions are derived from the two observation networks shown in Figure 1.

The borehole data are a network of 179 wells providing point estimates of each geological layer's thickness, hydraulic conductivity (required for the NNK method), and head and concentration for each geologic layer. The head and concentration values are interpolated to provide an initial condition representing the state of the system in 1992. The least-squares or LS data set is an alternative set of 180 observation wells that provide a temporal record of head and chloride concentration for each of the five aquifers over a period-of-record (POR) extending from 1992 to 2002. Observation wells near the model boundaries reveal a decline in pressure head in the I Aquifer over the POR, a trend that is reflected in the Dirichlet conditions. The head and concentration measurements that make up the LS data set are used in the second transport calibration phase. As can be seen in Figure 1, the borehole and LS data sets are not mutually exclusive. The borehole data are relatively sparse while the LS data are clustered around the injection well barrier.

The open-source groundwater model, FEMWATER version 3 (Lin *et al.*, 1997), meets all the modeling requirements for this study, and is adopted to solve the coupled flow and mass transport model defined in Equations 1 through 9. The finite element numerical procedure for solving the mathematical model is implemented in FEMWATER to generate solutions of head and concentration allowing either a coupled or an uncoupled flow and transport simulation (Lin *et al.*, 1997). An iterative successive-over-relaxation scheme is used to couple the flow and transport equations within each time step. Before proceeding with model development, a brief validation exercise was carried out with FEMWATER. The modified Henry's problem was simulated and model output was in excellent agreement when comparing with the semianalytical solution from Simpson and Clement (2004).

A pre- and post processing software package is used to aid in the development of the finite element mesh and in visualizing model output. To build the finite element (FE) model, the following procedure is followed. First, a plan view map is imported and the model boundaries are outlined. Discretization along the model boundary is course, on the order of a few hundred feet, and is successively tightened approaching the barrier where computational nodes are separated by tens of feet. Once a two-dimensional FE mesh is generated the mesh is copied and interpolated to the borehole data thereby defining the interfaces between each aquifer and aquitard. Then each aquifer is divided into three sections for a total of 19 FE layers in the conceptual model as shown in the schematic on the right side of Figure 3. Also shown a rendered view of the model containing 100,000 nodes that make up 188,119 three-dimensional finite elements is presented in Figure 3.

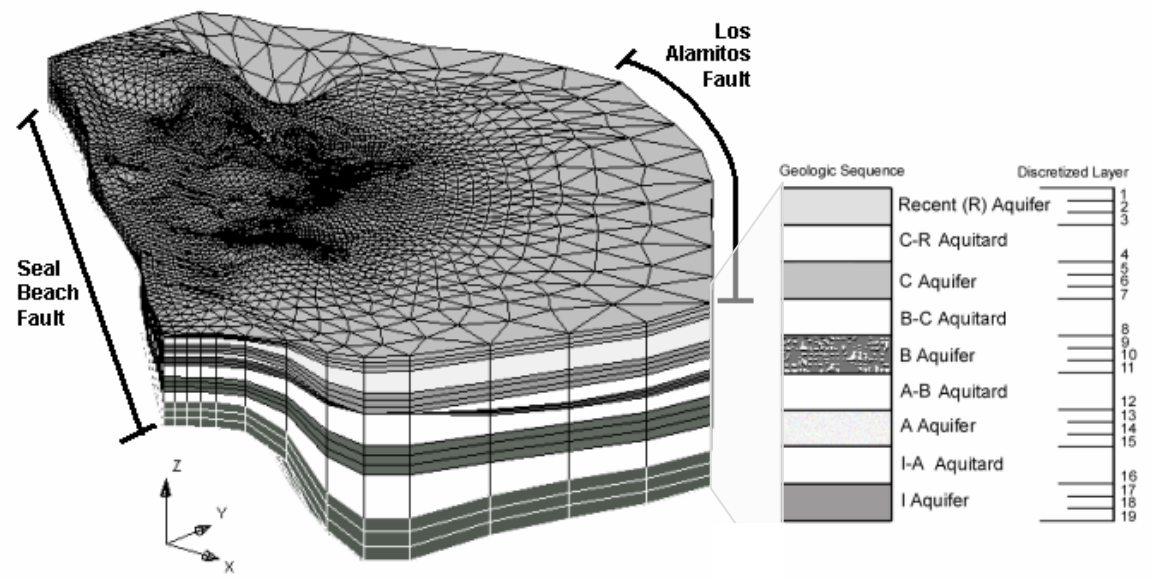

Figure 3: Rendered 3D View of ABP Conceptual Model with Aquifers Shaded and Aquitards Lightly Colored and Layer Sequence Schematic. Note z-dimension is exaggerated by a factor of ten.

Two-phase Calibration Procedure

In this study the flow and transport parameters are estimated in two independent, successive phases rather than a single unified approach primarily because of data availability. A geostatistical method, NNK, is developed to estimate the hydraulic conductivity field because a more extensive database of prior point estimates is available. In contrast, the transport parameters, α_L and α_T, are estimated by minimizing a measure of model fit, the least-squares error for concentration (LSE-CON). By separating the estimation of the predominant parameters of the two models, it is implicitly assumed that the crossover effect is negligible. Later in the calibration analysis the impact of the transport parameters on the least-squares error for head (LSE-HEAD) is investigated to verify this assumption.

Phase I: Estimation of the Hydraulic Conductivity Field

Kriging is a geostatistical method originally developed to estimate the extent of underground ore deposits by providing a reliable means of extrapolating a network of ore density measurements (Royle *et al.*, 1980). In a broader sense, the field of geostatistics arose from a need to explain how a particular regionalized random variable might vary as a function of location. Variations of the kriging method have been extended to geohydrology, particularly to estimate the heterogeneity of hydraulic conductivity (or transmissivity) since the parameter is highly correlated with local geological conditions (Yeh, 1986). One relevant example is a study by Li and Yeh (1999) that demonstrated the use of one kriging algorithm, named cokridging, as a means of solving the inverse problem for both coupled flow and transport models.

The proposed natural-neighbor-kriging (NNK) method is a variation of the kriging method, which estimates a parameter at an unsampled site using natural neighboring measured parameter values in the random field. In NNK, the natural neighbors of an unsampled site are determined based on Voronoi tessellation or Delunay triangulation (Tsai and Yeh, 2004), and represent the most influential data points to an estimate (Tsai *et al.*, 2005). NNK integrates standard kriging with a localized parameterization scheme called the natural-neighbor interpolation (NN) method (Sibson, 1981). An important distinction between the NN method in Tsai *et al.*, (2005) and NNK developed in this study is that in the former, the location and magnitude of the parameter values are considered as decision variables in an experimental design context.

In this study, an extensive network of observation wells (borehole data in Figure 1) provides a collection of point estimates of the hydraulic conductivity for each aquifer layer. The borehole data set is the necessary input needed to execute the NNK algorithm outlined in the five steps below. Steps 1, 2, and 5 are common among kriging algorithms, whereas steps 3 and 4 are adapted from the natural-neighbor parameterization scheme described in Tsai *et al.*, (2005).

1. Transform the borehole conductivity data by taking the natural logarithm. Calculate the spatial statistical properties (mean, covariance, and correlated length) of the transformed hydraulic conductivity data. Apply the transformation equation (shown below) to all borehole data (*NB=179*) for each aquifer layer (*NAL=5*):

$$Z_{i,j} = \ln\left(K_{i,j}\right), \quad i = 1,...,NB \quad j = 1,...,NAL \tag{10}$$

2. Develop experimental semivariograms for each of the five aquifers considered (R, C, B, A, I). Calculate the experimental semivariogram with the following expression from Journel and Huijbregts (1978, pp 12):

$$\gamma\left(M\right) = \frac{1}{2N\left(M\right)} \sum_{i=1}^{N(M)} \left[Z\left(x_i\right) - Z\left(x_i + M\right)\right]^2 \tag{11}$$

In Equation 11, *N(M)* is the number of experiment pairs of data separated by the distance *M* or [$Z(x_i)$,$Z(x_i+M)$]. Develop the experimental semivariogram using at least 25 pairs at each lag *M*. Then, apply a standard non-linear regression to develop a smoothed semivariogram fit to the experimental semivariogram. For the nonlinear regression, use the exponential semivariogram model below:

$$\gamma\left(M\right) = p_2\left(1 - e^{-3\left(\frac{M}{p_1}\right)}\right) \tag{12}$$

Equation 12 describes the variability of $\ln(K)$ for the five aquifers where γ is the semivariogram as a function of the distance lag *M*, and the two model parameters, p_1 and p_2, are estimated for each of the five aquifer layers.

3. Define the natural-neighbors by applying Voronoi tessellation (or Delaunay triangulation) to identify the unique set of polygons using the transformed borehole observation data set as the basis point locations (Tsai and Yeh, 2004).

4. Assign the natural neighbors for unsampled sites in the model domain (each computational element) not labeled in step 3.

5. Estimate $\ln(K)$ for each unsampled site by forming and solving the appropriate system of kriging equations. The general forms of the kriging equations with a non-stationary mean are presented below (Olea, 1999) and require the natural-neighbor index sets from steps 3 and 4 above.

$$\hat{Z}(\mathbf{x}) = \sum_{i=1}^{NN} \lambda_i Z_i \tag{13}$$

$$\phi(\mathbf{x}) = \sum_{l=0}^{n} b_l f_l(\mathbf{x}) \text{ and } f_0(\mathbf{x}) = 1 \tag{14}$$

$$\sum_{i=1}^{NN} \lambda_i(\mathbf{x}_0)\gamma_Y(\mathbf{x}_i, \mathbf{x}_j) - \mu_0 - \sum_{l=1}^{n} \nu_l f_l(\mathbf{x}_j) = \gamma_Y(\mathbf{x}_j, \mathbf{x}_0),\ j = 1, 2, \cdots, NN \tag{15}$$

$$\sum_{i=1}^{NN} \lambda_i(\mathbf{x}_0) f_r(\mathbf{x}_i) = f_r(\mathbf{x}_0),\ \ r = 0, \cdots, n \tag{16}$$

In Equations 13 through 16, *NN* denotes the number of natural-neighbors in the summation, and γ is the estimated or smoothed semivariogram (from step 2, Equation 12). Equation 13 is the standard kriging estimator equation which defines the estimated parameter value, $Z(\mathbf{x})$, with location vector $\mathbf{x}$, as a weighted sum of the neighboring parameter measurements. Finally, Equations 15 and 16 are effectively solved to estimate the conductivity for each element within each aquifer layer.

Equation 14 is a general expression for the drift representing first order non-stationarity. The residual is defined by $Y(\mathbf{x}) = \hat{Z}(\mathbf{x}) - \phi(\mathbf{x})$ and is assumed to be intrinsic, which therefore allows the residual semivariogram, γ_Y, in Equation 15, to be estimated easily. Usually the drift is assumed to be constant (first order stationary) especially for small or relatively homogeneous formations (Royle *et. al.*, 1980). In this case, the drift functions are zero and the residual semivariogram, γ_Y, is replaced in Equation 15 by the semivariogram γ determined in step 2 (Olea, 1999). In general, Equations 15 and 16 represent a system of linear equations that are solved to obtain the optimal kriging weights, λ_i, and Lagrange multipliers, μ_0 and ν_l. Once the optimal kriging weights are attained, Equation 13 is used to estimate the parameter for each computational element in each aquifer.

An advantage of the proposed NNK method is that it is computationally more efficient than a standard kriging algorithm, because in the latter all $\ln(K)$ measurements would be used in generating the linear equations and linear coefficients in Equation 15. Under the standard approach there would be a much larger number of equations and unknown coefficients that, when solved, provide a means of estimating the $\ln(K)$ anywhere in the domain. For a large-scale random field, this may not be necessary. In NNK, only a small subset of the $\ln(K)$ measurements is selected. In fact, a handful of the closest measurements are selected, which leads to a smaller set of linear equations and unknowns that can be solved faster and more efficiently. The second benefit of using

a subset of local measurements is that the estimation locations are close to the sample locations and in the high correlation region of the semivariograms.

In cases where prior data may be lacking in significant portions of the domain – or whether the data are simply too sparse – optimization may be used to improve upon the heterogeneous conductivity fields. The pilot point method (RamaRao *et al.*, 1995), for example, could be implemented where additional synthetic conductivity measurements can be optimized sequentially, in terms of location and magnitude, while constraining these points to respect the spatial statistics computed from the set of prior parameter measurements. In this study, optimization is not used to adjust the conductivity fields further because of adequate sampling density, especially in proximity to the injection barrier.

Phase II: Estimation of Transport Parameters

In the second calibration phase the key transport parameters are estimated. These are the longitudinal and transverse dispersivities, α_L [m] and α_T [m], which are determined such that the modeled concentration optimally matches the observed chloride concentration at the various observation data locations (LS data in Figure 1). Also, α_T is constrained to be one-tenth the value of α_L, which reduces by half the degrees-of-freedom in the optimization. The following procedure is implemented to determine the optimal values for α_L and α_T. To be clear, α_L and α_T are assigned as constant values to all nine geologic layers during this calibration phase. However, in the last step, step 6, four additional simulations are performed by systematically increasing and decreasing the optimized longitudinal and transverse dispersivities for the most sensitive A and I Aquifers. The upper bound of the parameter set is determined from the relationship between dispersivity and problem scale presented in Gelhar *et al.*, (1992).

1. Compile the head and concentration database (LS data) for the POR 1992 to 2002. Also, collect all pertinent data for injection and extraction wells within the problem domain.

2. Begin by setting the transport parameters to their lower bound, α_L = 0.10 ft (0.03 m) and α_T = 0.01 ft (0.003 m). Then perform a series of hot start simulations, slowly increasing the parameter a_2 in Equation 7 until reaching the appropriate value for chloride where $a_2 = 0.8013$ ft^{3}slug^{-1} (1.56x10^{-3} m^{3}kg^{-1}).

3. Simulate the POR with a reasonably small time step (Δt = 1 day) then compute and store the LSE-CON and LSE-HEAD by combining the modeled concentration and head to similar data from the LS database as in the LSE equations below:

$$\text{LSE-CON} = \sum_{i=1}^{NC} \left(C_i^* - C_i^0 \right)^2 \tag{17}$$

$$\text{LSE-HEAD} = \sum_{i=1}^{NH} \left(h_i^* - h_i^0 \right)^2 \tag{18}$$

In Equations 17 and 18, the superscripts "*" and "0" represent the modeled and measured variables, respectively.

4. Parametrically increase the transport parameters α_L and α_T and repeat step 3 until reaching the upper bound when α_L = 150 ft (46 m) and α_T = 15 ft (4.6 m).

5. Once at the upper bound of the parameter range plot LSE-HEAD and LSE-CON as a function of α_L. Determine the values of α_L and α_T that minimize LSE-CON and investigate the sensitivity of LSE-HEAD to changes in α_L and α_T.

6. Determine if the LSE-CON can be reduced further by slight modifications to the dispersivity assigned to the A and I Aquifers. Perform four additional runs where the dispersivity is decreased and increased systematically by 10% of the optimized value for both the A and I Aquifers while holding all other layers at the optimized values determined in step 5. Calculate the LSE-CON for each of the four additional runs and compare to LSE-CON from step 5.

   RUN 6-A: All aquifers set to α_L^* and α_T^* from step 5, except elements associated with the A Aquifer where α_L and α_T are decreased by 10%.
   RUN 6-B: All aquifers set to α_L^* and α_T^* from step 5, except elements associated with the A Aquifer where α_L and α_T are increased by 10%.
   RUN 6-C: All aquifers set to α_L^* and α_T^* from step 5, except elements associated with the I Aquifer where α_L and α_T are decreased by 10%.
   RUN 6-D: All aquifers set to α_L^* and α_T^* from step 5, except elements associated with the I Aquifer where α_L and α_T are increased by 10%.

Management Approaches

Phase III: Optimal Scheduling Problem (OSP)

The OSP is concerned with determining the optimal injection rates for each existing well along the barrier. The location and screened interval of each injection well represented in the simulation model is fixed and known. Gorelick (1983) reviewed distributed parameter groundwater management modeling methods concerning the joint use of groundwater simulation models and optimization methods and defined two broad categories of management models: groundwater policy evaluation and allocation models, and groundwater hydraulic management models. In the case of groundwater hydraulic management models, the decision variables are pumping or injection well rates, and are generally determined by one of two approaches, the embedding approach or the response matrix method.

In the embedding approach, the finite difference or finite element equations representing the simulation model are incorporated directly into the optimization formulation as equality constraints (*e.g.* Willis and Liu, 1984; and Shamir *et al.*, 1984). The primary disadvantage of the embedding approach is the large number of equality constraints added to the optimization formulation. In the response matrix method the

simulation model is represented by a response matrix, which has a smaller dimension. The basic procedure consists of the following four steps: first an initial policy is developed; second the response matrix is evaluated upon the initial policy; third the policy is updated by applying a specific optimization algorithm; and finally convergence criteria are examined. Iteration between the second and third steps is required for nonlinear management formulations or nonlinear simulation models like the unconfined flow or coupled flow and transport models.

While there have been many published variations of the response matrix method, also referred to as the influence coefficient method or sensitivity method, nearly all of them follow the same four basic steps outlined above. Becker and Yeh (1972) presented an iterative influence coefficient algorithm to estimate hydraulic parameters in a nonlinear open channel flow model. Louie *et al.* (1984) similarly adopted an iterative influence coefficient scheme in their study of a basin-wide management plan for a region in Southern California using a multiobjective management formulation. The recent study by Reichard and Johnson (2005) also implemented an iterative influence coefficient method to determine the least-cost water distribution scheme for a regional unconfined flow model of the Los Angeles County Basin.

One particular optimization software, the Modular In-core Nonlinear Optimization Solver (Murtagh and Saunders, 1995), or MINOS, has become very popular in applications of the response matrix algorithm. Gorelick *et al.* (1984) linked MINOS with the two-dimensional flow and transport model SUTRA to identify optimal aquifer reclamation designs. Willis and Finney (1988) developed a planning model for optimal control of seawater intrusion, comparing a quadratic programming model allied with the iterative influence coefficient method from Becker and Yeh (1972) with the reduced gradient quasi-Newton algorithm in MINOS. Finney *et al.* (1992) linked a quasi three-dimensional sharp interface model with MINOS to identify optimal pumping policies that limit seawater intrusion for a multilayerd aquifer system in Jakarta. Emch and Yeh (1998) linked MINOS with the sharp interface flow and transport model SHARP to examine optimal conjunctive use strategies in a multiobjective formulation for the Waialae Aquifer in Southeastern Oahu. Important to note, as recognized by Willis and Finney (1988), is that only locally optimal solutions can be guaranteed for a nonlinear objective and non-convex constraints; and furthermore, the optimal solutions obtained by coupling nonlinear solvers with complex groundwater simulation models tend to be computationally intensive and sensitive to the specified initial policy.

Two alternative OSP formulations are investigated, the hydraulic gradient control (HG), which is combined with post optimization analysis, and the combined hydraulic and transport formulation (CHT). The HG formulation is presented below.

$$\min_{\mathbf{q}} \quad \sum_{t=1}^{NT}\sum_{i=1}^{NW} q_{i,t} \tag{19a}$$

$$\text{s.t.} \quad h_{j,NT}(\mathbf{q}) \geq H_j, \quad j = 1,...,NL \tag{19b}$$

$$0 \leq q_{i,t} \leq QM_{i,t}, \quad i = 1,...,NW;\ t = 1,...,NT \tag{19c}$$

The OSP objective function defined in Equation 19a is to minimize the total injected water over all *NW* injection wells and *NT* management periods. The objective function is linear in terms of the decision variables, which are the injection well rates $\mathbf{q} \in \mathsf{R}^N$, where *N=NW*NT*. In the HG formulation above, only one type of nonlinear constraint is considered, Equation 19b, the end-of-period (EOP) minimum head targets at *NL* target locations. In Equation 19b, $h_{j,NT}$ is the predicted EOP head (obtained from the calibrated simulation model) at the j^{th} target location, and H_j is the lower bound on the hydraulic head at the j^{th} location. Equation 19c defines the operational minimum and maximum injection rate, $\mathbf{QM} \in \mathsf{R}^N$, that can be assigned to each injection well in each management period. In the HG formulation the total number of decision variables is *N* and the total number of nonlinear constraints is *M=NL* with 2*N* box constraints placing upper and lower bounds on the injection rates.

Since the HG formulation only involves nonlinear constraints on the hydraulic head, only the solution of the groundwater flow equation is necessary. Following optimization, however, additional simulations of the coupled flow and transport model are conducted to investigate the optimal hydraulic policy performance in terms of meeting chloride concentration targets.

The CHT formulation includes constraints on both hydraulic head and chloride concentration. Note that the objective and operational constraints on the injection wells are common among both the HG and CHT shown below.

$$\min_{\mathbf{q}} \quad \sum_{t=1}^{NT}\sum_{i=1}^{NW} q_{i,t} \tag{20a}$$

s.t.
$$h_{j,NT}(\mathbf{q}) \geq H_j, \quad j = 1,...,NL_1 \tag{20b}$$

$$c_{j,NT}(\mathbf{q}) \leq C_j, \quad j = 1,...,NL_2 \tag{20c}$$

$$\frac{1}{NT}\sum_{t=1}^{NT} h_{j,t}(\mathbf{q}) \geq \eta_j, \quad j = 1,...,NL_3 \tag{20d}$$

$$\frac{1}{NT}\sum_{t=1}^{NT} c_{j,t}(\mathbf{q}) \leq \chi_j, \quad j = 1,...,NL_4 \tag{20e}$$

$$0 \leq q_{i,t} \leq QM_{i,t}, \quad i = 1,...,NW; t = 1,...,NT \tag{20f}$$

The first two sets of (nonlinear) constraints, Equations 20b and 20c, are the EOP minimum head and EOP maximum concentration targets at NL_1 and NL_2 target (node) locations, respectively. Clearly the equivalent objective function is applied in both formulations (compare Equation 20b with Equation 19b). In Equation 20c, $c_{j,NT}$ is the predicted EOP concentration at the j^{th} target location and C_j is the maximum concentration target at the j^{th} location. The second set of nonlinear constraints, represented by Equations 20d and 20e, are added to maintain the mean head and mean concentration above a specified target level. In Equation 20d, η_j is the specified mean head target at the j^{th} location, and χ_j is the mean concentration target in Equation 20e. Reichard and Johnson (2005) also used a mean head constraint similar to Equation 20d in their formulation to discourage large fluctuations in the injection rate over successive management periods.

In the CHT formulation, Equations 20a to 20f, the total number of decision variables is the same as the HG formulation, $N=NW*NT$; however, the total number of nonlinear constraints is now $M=NL_1+NL_2+NL_3+NL_4$. Also there are still $2N$ box constraints defined in Equation 20f, which ensure operational feasibility of the decision variables. In order to solve formulations presented above, the simulation model is allied with MINOS, which solves nonlinearly constrained optimization problems by solving a series of subproblems, each minimizing an augmented Lagrangian with linearized constraints using a quasi-Newton method (Murtagh and Saunders, 1995).

The first two scenarios are simulated in a historical mode in order that optimal policies can be compared to historical operation. In the third scenario the simulation-optimization framework is used to specify a future injection policy that will improve upon current barrier conditions.

Scenario 1: Steady Optimal Scheduling Problem, Historical Mode: In this scenario the HG formulation in Equations 19a to 19c is adopted. The simulation model is run for eleven years spanning the calibration period-of-record (POR) from 1992 to 2002 with an annual simulation time step. However, in this case a single or steady injection rate is considered for each well over the POR, therefore $NW=43$, $NT=1$, and $N=43$ in Equation 19a. The right-hand-sides of Equation 19b are determined by a base simulation run assigning the mean recorded injection rates to each well over the POR and tabulating the resultant EOP head at NL target locations. Two optimization runs are performed to examine the sensitivity to the initial policy, and the optimized results in both cases are compared to the historical record. Post optimization analysis examines the optimal policy's performance in terms of meeting the transport targets explicitly defined in the CHT formulation.

Scenario 2: Transient Optimal Scheduling Problem, Historical Mode: The second scenario is a transient extension where injection rates now vary on an annual basis over a five year POR extending from 1998 to 2002. In this case $NT=5$ and $NW=43$, therefore the total number of decision variables are $N=215$. Both the HG formulation in Equations 19a to 19c and the CHT formulations in Equation 20a to 20f are considered. When operating under the historical mode, a baseline simulation run is performed assigning to each well the recorded mean annual injection rates and using head and concentration output to assign the head and concentration targets of the nonlinear constraints. Optimal transient injection policies are compared to the recorded mean annual injection rates over the same period.

Scenario 3: Transient Optimal Scheduling Problem, Forward Mode: The HG formulation is adopted where the total injected water is minimized such that a majority of the head targets, specifically the right-hand-sides of Equation 19b, are increased by 5% over a five-year period. Similar to the previous scenario, five management periods are considered for the existing barrier configuration, therefore $N=215$.

Phase IV: Optimal Well Location Problem (OWLP)

The decision variables for the OWLP are the locations of a preset number of new injection wells, where the optimal locations are those that result in the biggest marginal improvement to the hydraulic gradient along the existing barrier alignment. The improvement is quantified as the gain in the head at target locations over a baseline that represents no additional wells. For the OWLP defined here, candidate locations for new injection wells are any node within a specified distance of the existing barrier alignment that is not already a target location for measuring the hydraulic improvement, or an existing injection well node. New wells are set to inject at an operational maximum consistent with existing injection wells and are screened over only one of the following four aquifers C, B, A, and I. All existing wells are set to the mean annual injection rate based on the historical data record during the OWLP optimization procedure.

A genetic algorithm is proposed to solve the OWLP. Optimal locations for new injection wells are identified by linking the open source GA by Carroll (2004) with the simulation model. The user is required to develop a problem specific chromosome encoding scheme and formulate a fitness function to evaluate chromosome performance.

Each chromosome is a binary string of numbers that represent one individual in a population of P individuals that comprise a single generation. Each GA iteration seeks to improve upon the fitness of the current population by the processes of selection, mating, crossover, and mutation of individuals within the population creating a new population of individuals. Figure 4 illustrates how a single chromosome string is decoded into one or more potential locations for new injection wells. The length of the chromosome, therefore, is determined both by the number of new wells added, and by the number of potential locations considered. In this study, the decoded chromosome specifies the spatial location and layer for the new injection well which is the key input driving the simulation model.

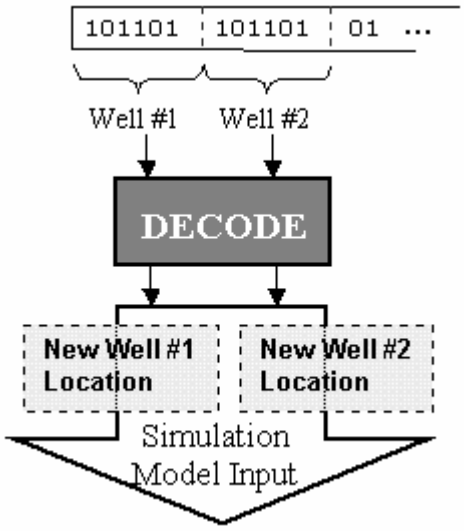

Figure 4: GA Chromosome Mapping Schematic.

Next the fitness function is developed to evaluate the performance associated with each individual chromosome. In this application, the fitness is defined as the marginal improvement in EOP head and mean head targets represented in the two terms below.

$$fitness_k = \omega_1 \sum_{j=1}^{NL_1} \left(h_{j,NT} - H_j \right) + \omega_2 \sum_{j=1}^{NL_2} \left(\frac{1}{NT} \sum_{t=1}^{NT} h_{j,t} - \eta_j \right), \quad k = 1, \ldots, P \tag{21}$$

The fitness for the k^{th} individual in a population of P individuals is the sum of the marginal gain in the EOP target and the mean head, which is derived by rearranging the nonlinear constraints in Equations 20b and 20d, respectively. Since these terms are dimensionally compatible the weighting coefficients ω_1 and ω_2 are set to unity.

The fitness function in Equation 21 links the decision variable, the locations of new injection wells, and the state variable, in this case head. The GA must be dynamically linked to the simulation model to evaluate the fitness for a given chromosome configuration. The primary disadvantage of the GA is that the algorithm is computationally intensive requiring repeated calls to the simulation model to evaluate the fitness of many individuals over successive generations. However, as suggested by Banzhaf *et al.* (1998), an effective way of accelerating the GA is to incorporate parallel processing. By evaluating the fitness of each individual in parallel, rather than in sequence on a single processor, a significant reduction in execution time is realized. The solution algorithm is presented in Figure 5. One processor is dedicated to carrying out the basic steps of the GA, with the exception of computing the fitness. An interface routine distributes the individual chromosomes to P processors where the chromosome is decoded, the simulation model is executed predicting the state variables **h**, and finally the fitness is calculated. The interface routine gathers the fitness values for all P individuals on the master node and continues with the GA. Only a minor addition of source code is required to convert the FORTRAN77 GA (Carroll, 2004) to a parallel configuration, and no modifications are necessary to the simulation model executed on parallel CPUs.

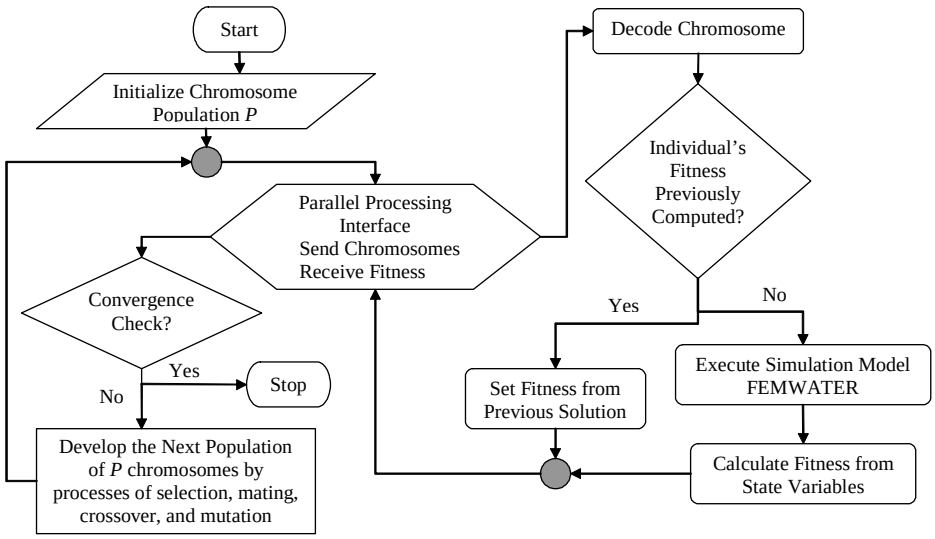

Figure 5: Optimal Well Location Problem Solution Algorithm.

While the decision variable for the OWLP is the location of new injection wells, reasonable limitations must be placed on the sites considered in the OWLP to ensure the problem is tractable and yields useful results. Candidate locations for new injection wells are limited to be within a specified distance of the existing barrier alignment. Any node within this distance is a candidate unless already representing existing injection wells, or designated for hydraulic target evaluation. A new injection well is screened over only one of the C, B, A, and I Aquifers, and each new well is defined by a single finite element node pair because the new well is screened over the entire aquifer's thickness. A

population of four individuals is considered, $P=4$, and the GA is terminated after 100 successive generations. The locations of two additional injection wells are determined from 1,978 candidates within 50 ft (15.25 m) of the existing barrier alignment.

Target Location Development for Nonlinear Constraints

An important aspect of both management problems is the location of target sites. Preliminary simulations indicate that at least one target must be near each injection well otherwise the well will be set to the nontrivial minimum injection rate during optimization. Therefore, a set of target locations is determined using nodes in close proximity to one or more of the existing injection wells to ensure sensitivity among decision variables and state variables.

Figure 6 is a plan view of 178 target nodes to be used in the optimization formulations. In the HG formulation, all 178 target sites are dedicated to the EOP head targets in Equation 19b, therefore $M=NL_1=178$. In the CHT formulation, the target locations are divided into two equal groups such that half of the target locations are assigned to the EOP constraints where $NL_1=NL_2=89$ in Equations 20b and 20c, and the other half are assigned to the mean constraints where $NL_3=NL_4=89$ in Equations 20d and 20f, for a total of $M=356$ nonlinear constraints.

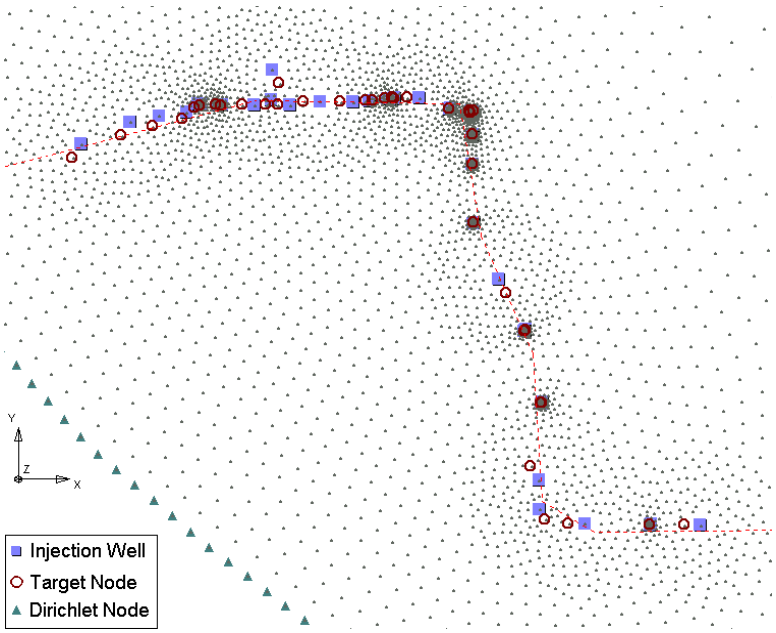

Figure 6: Injection Wells and Target Locations for Nonlinear Constraints Along the Barrier Alignment.

RESULTS

Hydraulic Conductivity Parameterization

After transforming the borehole conductivity data via Equation 10, the semivariograms are developed for each aquifer layer under the assumption of a first order stationary mean. For each semivariogram, a standard nonlinear regression is applied to

estimate the parameters p_1 and p_2 in the semivariogram model (Equation 12). Carrying out the remaining steps finally leads to the estimated $\ln(K)$ for all elements within each of the five aquifers. Each aquitard is assigned a homogeneous hydraulic conductivity several orders of magnitude lower than the hydraulic conductivity in the aquifers, except in mergent areas where the hydraulic conductivity is modified to match the appropriate layer. Figures 7a to 7e are the smoothed contour plots of the five heterogeneous hydraulic conductivity fields with each semivariogram inset in the upper right corner. The greatest variation in hydraulic conductivity is evident in the uppermost and lowest R and I Aquifers, respectively. The R Aquifer exhibits a wider cardinal range in the conductivity parameter as evidenced by the hydraulic conductivity statistics in Table 1, which exhibits the minimum, mean, maximum, and standard deviation for each of the nine geologic layers: five aquifers and four aquitards in the order they are presented in Figure 3. These statistics are computed over the set of numerical elements in a single computational layer corresponding to one of the nine geologic layers. Note that the aquitard statistics do not reflect a homogeneous layer because of mergent areas within their domain. The mergent zones in the C, B, and A Aquifers tend to reduce significantly the hydraulic conductivity near the south-west (Seal Beach Fault) boundary.

A common feature among the five heterogeneous plots in Figures 7a through 7e is local circular zonation trends of low or high hydraulic conductivity. The overall trends in the hydraulic conductivity and topology of each of the five aquifer layers is consistent with those presented by Callison *et al.* (1991). However, the estimated hydraulic conductivity field by NNK contains much more variability than those from the previous study. Local variability of the hydraulic conductivity is important as the model is intended to be used for optimizing the operation of the Alamitos Barrier Project. Before DD simulations are conducted, the heterogeneous hydraulic conductivity fields are converted to intrinsic permeability via Equation 4.

Table 1: Hydraulic Conductivity Statistics for Each Geologic Layer [ft/day].

Layer	Min	Max	Mean	Std Dev
I	33.601	459.93	155.40	51.82
C-I	0.026	45.99	0.93	3.38
C	0.283	459.93	113.43	47.59
B-C	0.028	19.14	0.21	1.23
B	5.669	245.62	83.88	37.95
A-B	0.567	8.93	0.63	0.59
A	$9.0\text{x}10^{-5}$	998.16	163.45	54.51
I-A	$9.0\text{x}10^{-6}$	8.93	0.06	0.64
I	25.676	276.14	98.96	35.41

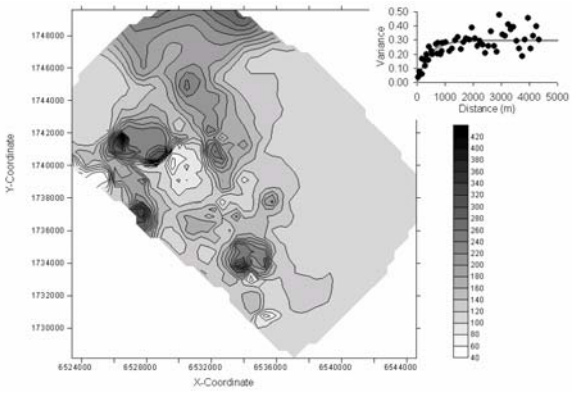

(a)

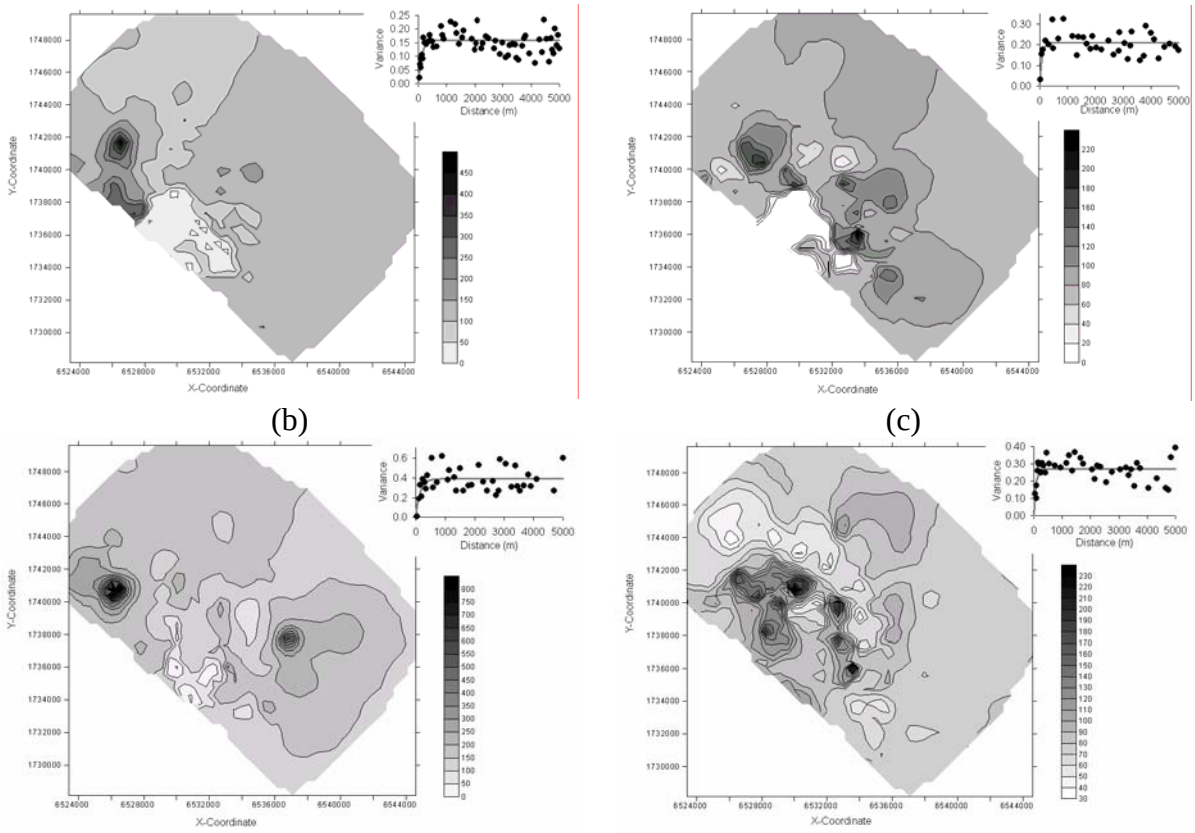

Figure 7: Heterogeneous Conductivity Distribution (ft/day) for Each Aquifer Layer with Semivariogram Inset. (a) R Aquifer; (b) C Aquifer; (c) B Aquifer; (d) A Aquifer; (e) I Aquifer.

Transport Parameterization

An extensive database of head and chloride concentration is available from LACDPW and has been introduced as the LS data plotted in Figure 1. The LS data consists of 180 observation wells providing *NH* = 2,297 and *NC* = 4,221 over the calibration POR (1992 to 2002). As can be seen in Table 2, the number of concentration data outnumbers the head data because a maximum of three measurements are possible at different depths within a single geologic layer tapped by the observation well where only a single corresponding head measurement is recorded. A data set of all injection and extraction rates for each well operating in the study area also is provided by LACDPW for this phase of the calibration.

Table 2: Least-Squares Data Set Measurement Breakdown

Aquifer	Number of Wells	Measurement Tally	
		P. Head	Conc.
R	35	343	493
C	20	300	500
B	27	357	496
A	52	685	1,458
I	46	612	1,274
Totals	180	2,297	4,221

First, the transport parameters are set to their lower limit: α_L = 0.1 ft (0.03 m) and α_T = 0.003 m (0.01 ft). Then twenty hot start simulations are executed, simulating only a few daily steps for each simulation as the parameter a_2 (from Equation 7) is gradually

increased up to 1.56×10^{-3} $m^3 kg^{-1}$, appropriate for chloride which corresponds to a maximum fluid density of 999 kg/m^3. After adjusting the initial conditions based on the hot start simulation results, nine calibration runs are performed gradually increasing α_L (ft) in the sequence: 0.1, 1, 5, 10, 20, 35, 50, 100, 150. Recall that the transverse dispersivity is constrained to one-tenth of the assigned longitudinal value. The eleven year POR is simulated with a time step of one day leading to an average run time of 12 days per simulation on a Dell Pentium IV with two GB of DDR RAM. Larger time steps, while reducing simulation time, led to a notable increase in numerical dispersion, therefore time steps are maintained at one day for all calibration runs. The LSE-CON and LSE-HEAD are computed with Equations 17 and 18 following each simulation and they are plotted respectively on a semi-Log scale in Figures 8a and 8b.

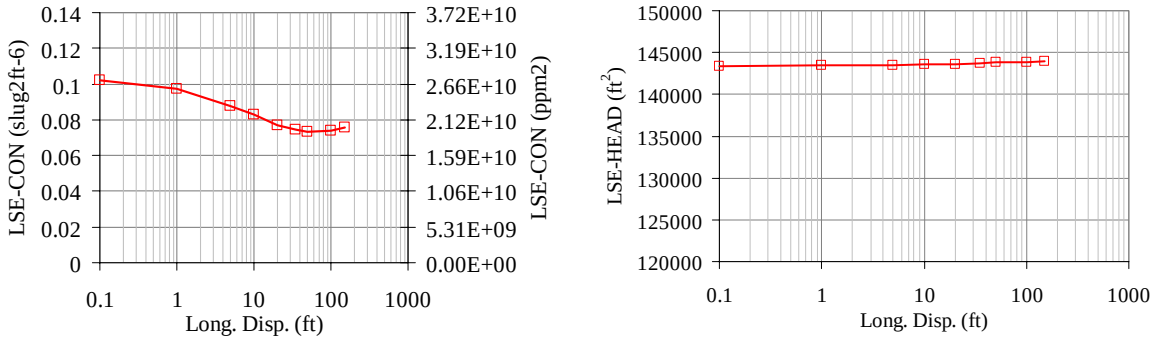

(a) (b)

Figure 8: Least-Squares Error Variation as a Function of Longitudinal Dispersivity for (a) Concentration (LSE-CON) and (b) Head (LSE-HEAD).

The LSE-CON decreases with increasing α_L until reaching a minimum of 1.95×10^{10} ppm^2 near α_L = 50 ft (15.2 m), then LSE-CON begins increasing with increasing α_L. The rate of change in LSE-CON given a change in α_L appears to decrease around the minimum. Figure 8b demonstrates that the LSE-HEAD is not sensitive to large variations in the transport parameters, supporting the assumption that the crossover effect is negligible for these parameters. For a three order of magnitude shift in α_L, LSE-HEAD increases slightly by 0.3%.

Four remaining simulations (described in Step 6 of the Phase 2 procedure) are executed in an attempt to further reduce the model error by a 10% variation in α_L and α_T for the most significant aquifers A and I. Table 3 presents the variation in aggregate LSE-CON for the baseline and additional runs, revealing only a slight change in model error for the variation considered. In fact, when looking only at the change in LSE-CON for the affected layer, a reduction of 0.14% is observed for the A Aquifer in the case when the dispersivities are decreased by 10%. The trend for the I Aquifer is reversed, however, where a decrease of 0.01% in LSE-CON is observed when the dispersivities are increased by 10%. The variation in LSE-HEAD is even less significant than LSE-CON for the additional simulations as evidenced by Table 3. In conclusion, the improvement in model error is insignificant by increasing dispersivity parameter complexity.

Table 3: Tracking the Least-Squares Error for Concentration and Head with 10% Variation in Dispersivities from Baseline.

Run ID	Longitudinal Dispersivity (ft)	LSE-HEAD $(m)^2$	LSE-CON $(ppm)^2$	Affected Layer
Baseline	50	143776.8	1.951E+10	None
6A	45	143774.7	1.950E+10	A-Aquifer
6B	55	143776.5	1.952E+10	A-Aquifer
6C	45	143777.7	1.950E+10	I-Aquifer
6D	55	143776.6	1.952E+10	I-Aquifer

Optimal Scheduling Problem Simulation-Optimization

Scenario 1 Results: Steady Optimal Scheduling Problem, Historical Operation

The first scenario is to determine the optimal steady injection rates for each of the injection wells by minimizing their sum, subject to the nonlinear EOP head targets defined in Equation 19b under the HG formulation. The EOP head targets were determined by solving the simulation model using the historical mean injection rates for each of the injection wells and the consequent EOP heads form the head targets for Equation 19b. It should be noted that the head constraints are all active and the corresponding policy is referred to as the "optimum" policy. Before the simulation-optimization model is executed, an initial injection policy that lies between the maximum and the optimum (the recorded mean injection rate) is developed for each well to begin optimization. Figure 9 shows the convergence of the objective function with successive nonlinear iterations for five alternative optimization runs each with a differing number of decision variables considered. When the decision variables are limited to ten or less, the objective decreases rapidly in the first iteration converging to a policy essentially equivalent to the global optimum. When the decision variables are increased to twenty wells, the convergence rate slows down and the global optimum is not attained. When the full barrier is considered (*NW=N=43*), the objective function could not be improved after 12 iterations in 170 hours (7 days) of runtime and a total of 1,207 calls to the simulation model converging to approximately $2.20*10^5$ ft^3/day ($6.24*10^3$ m^3/day), about 41% greater than the optimum value of $1.56*10^5$ ft^3/day ($4.43*10^3$ m^3/day).

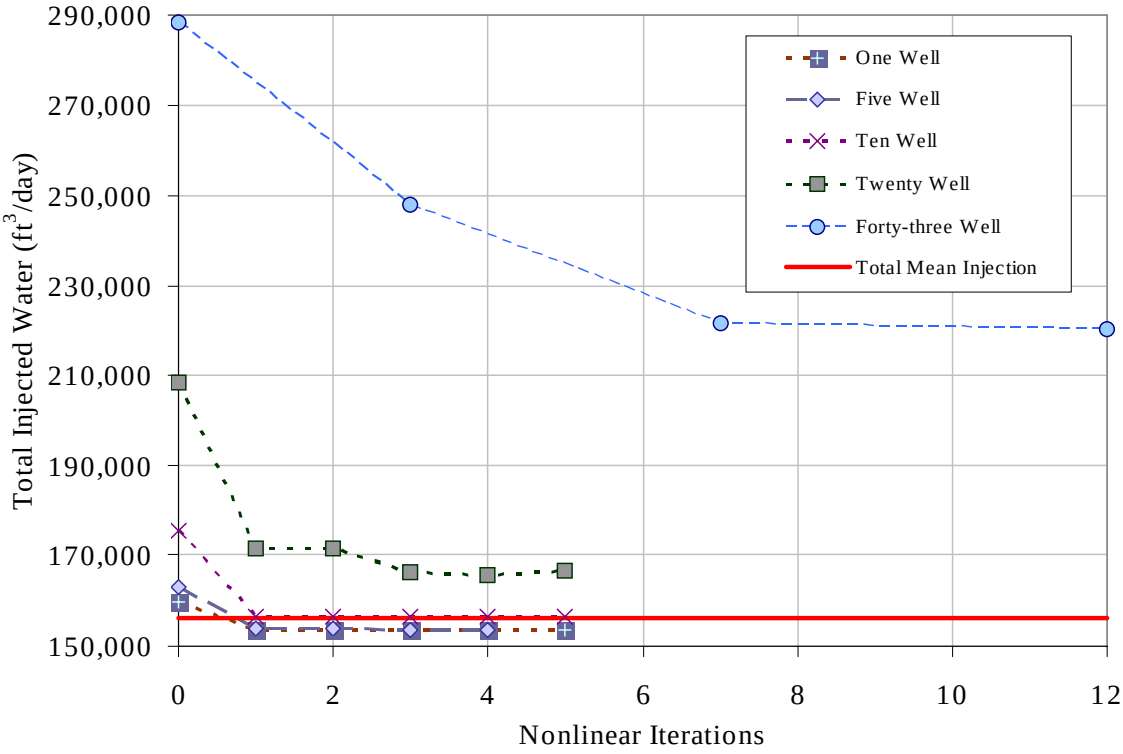

Figure 9: Optimal Scheduling Problem, Scenario 1 Steady Injection Objective Function Tracking with Nonlinear Iterations and Varying Number of Decision Variables.

Figure 10 presents for each well, the steady injection rate for the initial policy, the corresponding optimized policy, and the "optimum policy." Clearly the initial policy for each well is much greater than the historical mean injection rate. In terms of the optimized policy, most injection wells show improvement over the initial policy, injecting less water and in many cases approaching the optimum. For three wells 492BF, 502N, and 502AW, the optimized injection rate is greater than the initial policy. All of the nonlinear hydraulic gradient targets are satisfied, and only seven of 178 targets are active at their lower bound suggesting a further reduction of injected water is theoretically possible.

While Figures 9 and 10 demonstrate that the simulation-optimization model can significantly improve upon the assigned initial policy; these figures also imply that convergence to the global optimum may not be possible as the optimization problem is beset with nonlinearity as well as nonconvexity. A second simulation-optimization run is executed to examine the sensitivity to the initial policy. For the second simulation the initial policy is more ambitious reducing the steady injection rate closer to the optimum. Table 4 presents the results.

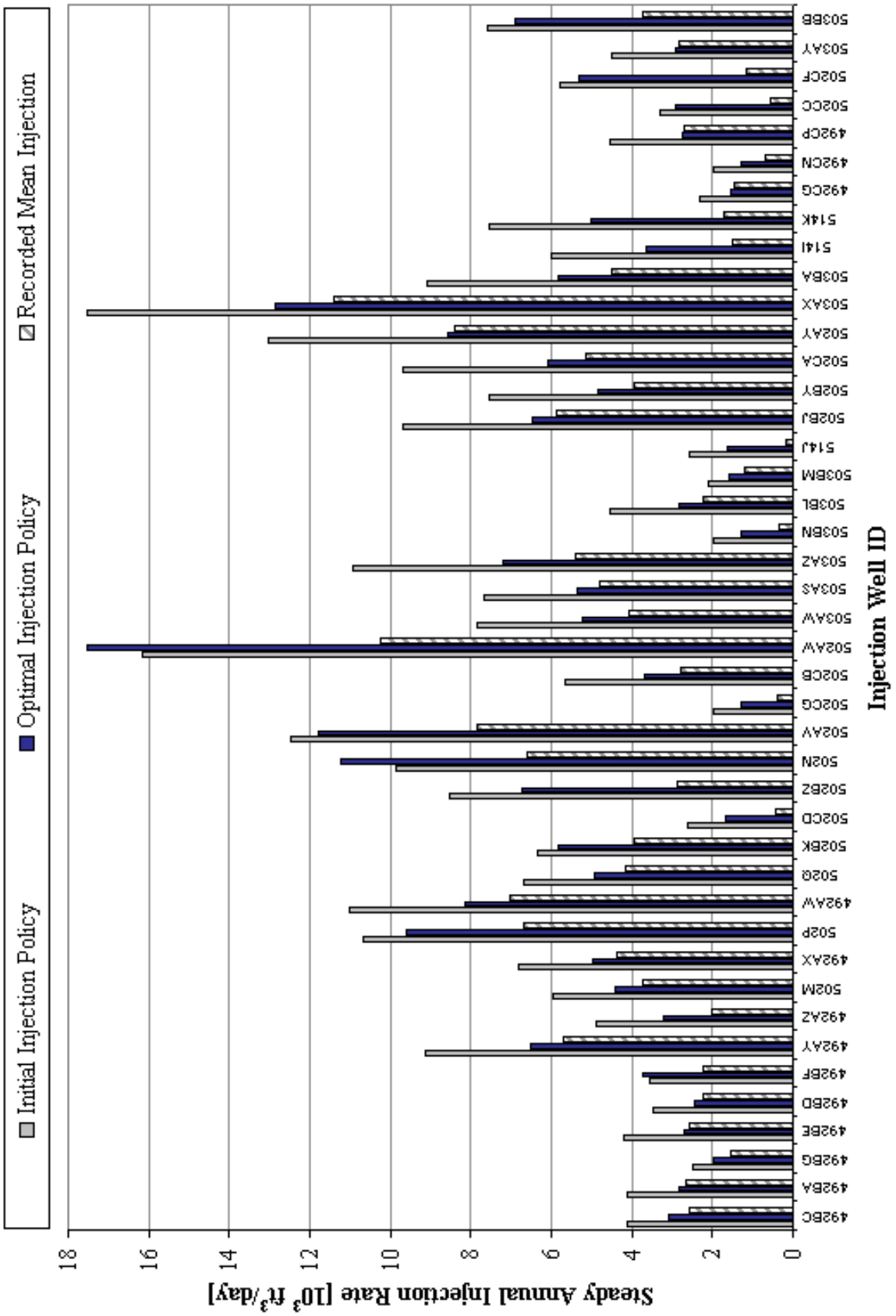

Figure 10: Optimal Scheduling Problem, Scenario 1 Steady-State Injection Results.

Table 4: Optimized Objectives for Steady Optimal Scheduling Problem with Two Alternative Initial Policies and the Total Recorded Water Injected.

Solution Method	Objective (ft^3/day)	Nonlinear Iterations	Execution Time (hr)
Optimized Solution with First Initial Policy	220,380	16	170.0
Optimized Solution with Second Initial Policy	176,039	4	104.6
Total Water Injected Based on Historical Record	156,413		

For the steady injection case, both simulation-optimization runs yielded an injection policy that is greater or more conservative in terms of meeting hydraulic targets. Furthermore, as demonstrated above, the optimized policy is clearly sensitive to the initial policy where a more ambitious initial policy in the second simulation converges to a lower objective function value. Before proceeding with the post-optimization analysis, the following abbreviations are adopted to distinguish between the two solutions associated with the two alternative initial policies. Let the optimized solution associated with the higher, conservative initial policy be referred to using the abbreviation IP-A, and the abbreviation IP-B is used to refer to the optimized solution associated with the second, more ambitious, initial policy.

Following optimization, a coupled flow and transport simulation is executed where each optimized policy is input to the simulation model, and hydraulic head and concentration are calculated at selected target locations. First, the hydraulic heads are successfully verified at each of the 178 EOP head target locations for both cases. Then the selected target locations are divided into two groups consistent with the approach adopted in the CHT formulation where half are assigned to the EOP head and concentration constraints ($NL_1 = NL_2 = 89$ in Equations 20b and 20c), and the other half assigned to the mean head and concentration constraints ($NL_3 = NL_4 = 89$ in Equations 20d and 20e). Following this convention, the EOP and mean hydraulic head constraints are next verified for both IP-A and IP-B. As expected, more of the nonlinear hydraulic constraints in both the EOP and mean head cases are active, at or very close to their lower limit. Next the EOP concentration constraints are calculated for both optimized policies and compared with the baseline. The abscissa of Figure 11 indicates the constraint index, and the elevation of the target locations generally decreases from left to right. Higher indices along the axis, therefore, correspond to targets in deeper aquifers.

Figure 11a shows that nearly all of the slacks associated with the EOP concentration constraint for IP-A are negative or very near 0 ppm. The maximum positive slack in Figure 11a is equal to 71 ppm and represents the maximal violation in the nonlinear EOP concentration inequality defined in Equation 20c. In the case of IP-B, the EOP concentration constraint slacks plotted in Figure 11b reveal three constraints are more blatantly violated with slacks equaling 534, 500, and 135 ppm. The two most significant violated constraints in Figure 11b are constraints 61 and 76, which are two targets on the southern end of the barrier alignment located in the I Aquifer indicating an elevated concentration in this region. Note that these two constraints could be made feasible by simply increasing the injection rate at the nearest injection well, well 503BN, until the concentration has been adequately reduced.

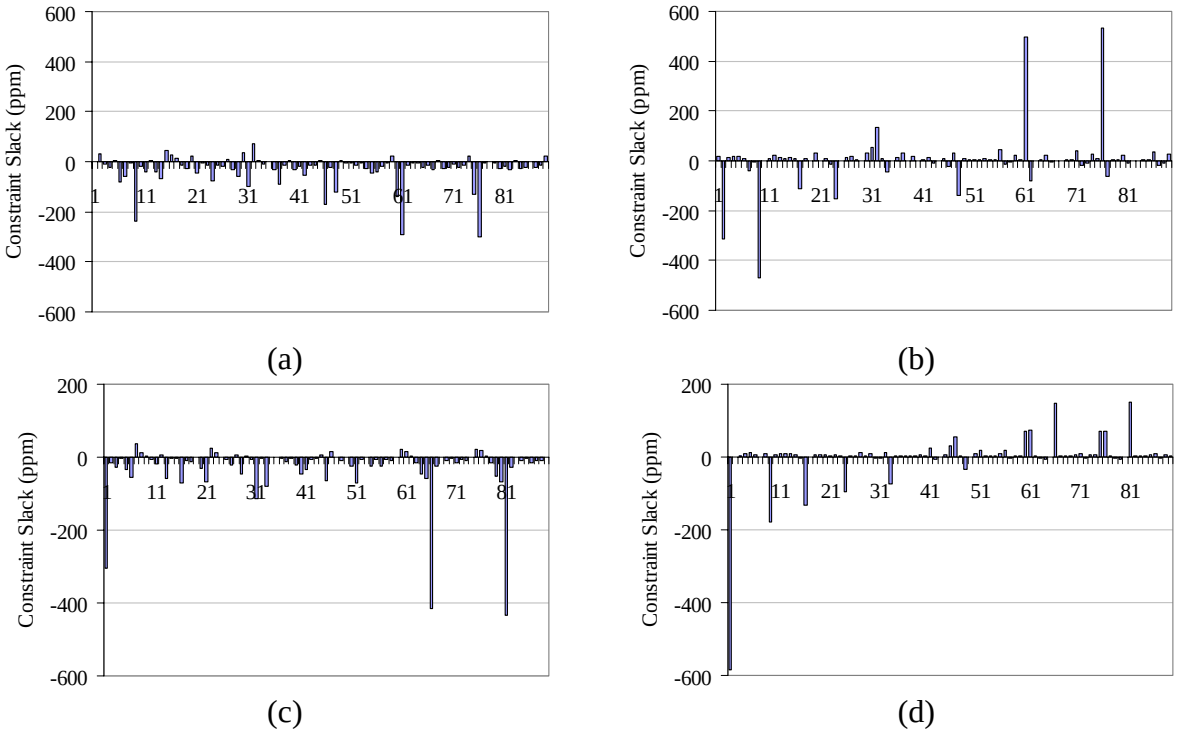

Figure 11: Nonlinear Constraint Slacks for (a) End-of-Period Concentration IP-A, (b) End-of-Period Concentration IP-B, (c) Mean Concentration IP-A, and (d) Mean Concentration IP-B.

The trends in the nonlinear constraint slacks comparing EOP concentration and mean concentration are generally consistent for a given initial policy, for example comparing Figure 11a with 11c or 11b with 11d. However, when comparing the trends associated with two policies (*e.g.* comparing Figure 11a with 11b or 11c with 11d), the slacks associated with IP-B generally varies from negative to positive from left to right along the abscissa. Recalling that constraints with a higher index are associated with relatively deeper aquifers, the positive trend in the slacks in Figure 11b and 11d infers that the optimized policy from IP-B shows a greater potential for seawater intrusion, particularly in the deeper aquifers. In contrast, the nonlinear constraint slacks in Figures 11a and 11c do not follow a similar trend; rather the distribution appears to be uniformly random, varying between small and large negative values along the abscissa. Therefore the optimized policy associated with the conservative initial policy (IP-A) is also conservative in that more water is injected, but also inferring a reduced potential for elevated chloride levels in the future.

Scenario 2 Results: Transient Optimal Scheduling Problem, Historical Operation

When transitioning from steady to transient optimization, the number of decision variables rapidly increases. Before all 43 injection wells are considered in the optimization, two of the 43 wells are optimized in order to compare the nonlinear approach under transient conditions to the historical record. These two injection wells, 502M and 502P, inject freshwater into both the A and I Aquifers. The CHT formulation in Equations 20a to 20f is adopted and a subset of 16 of the closest targets is selected for developing the nonlinear constraint set. Of the 16 target locations, one half are dedicated

to EOP head and concentration constraints (Equations 20b and 20c, respectively), and the other half are dedicated to mean head and concentration targets (Equation 20d and 20e, respectively). The total number of management periods in this test case is 11 years, therefore the number of decision variables is *N=2*11=22*, with a total of 32 nonlinear constraints ($NL_1 = NL_2 = NL_3 = NL_4 = 8$).

For the nonlinear two well test case, the initial policy for each well is to assign the maximum recorded injection rate uniformly over an 11 year period. The optimized total injected water for well 502M is $4.47*10^4$ ft^3/day ($1.27*10^3$ m^3/day), slightly less than the corresponding historical value of $4.48*10^4$ ft^3/day ($1.27*10^3$ m^3/day). For well 502P the improvement is more dramatic where the optimized total injected water equals $6.30*10^4$ ft^3/day ($1.78*10^3$ m^3/day) compared to $7.44*10^4$ ft^3/day ($2.11*10^3$ m^3/day) based on the historical record. Figures 12a and 12b show the optimized injection schedules with the corresponding historical mean annual injection rates for wells 502M and 502P, respectively. For this limited number of injection wells, the initial policy appears to have no influence on the optimized solution since the maximum injection is uniformly applied to each well prior to optimization; although there is clearly relatively less variation in the optimized mean annual injection rates compared with the historical injection rates.

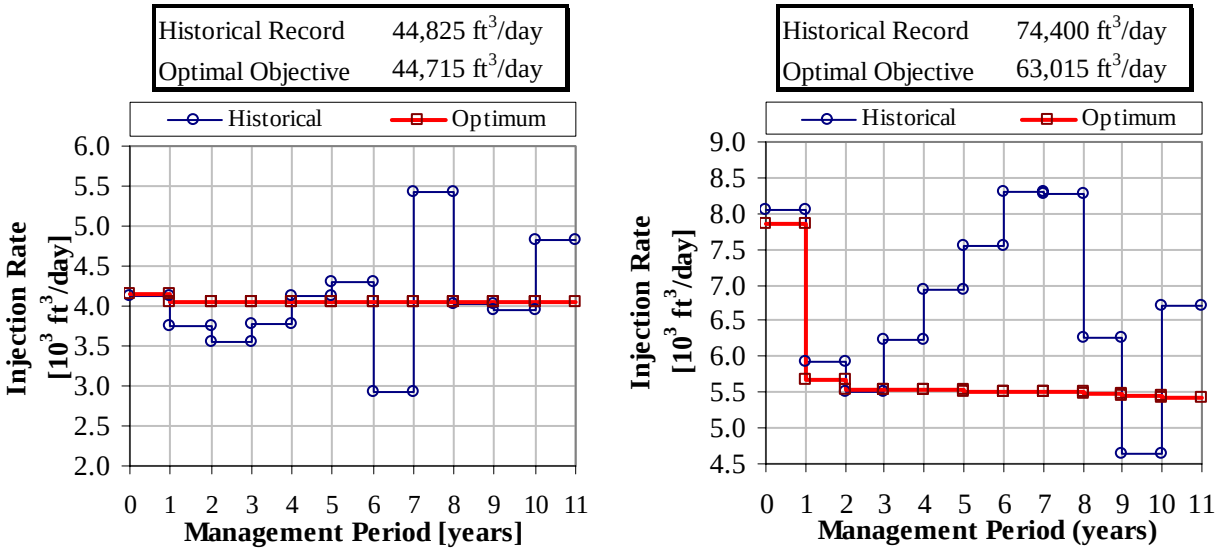

(a) (b)

Figure 12: Optimal Injection Schedules with Concurrent Historical Mean Annual Injection for Wells (a) 502M, and (b) 502P.

Next the simulation-optimization model is employed to optimize all 43 wells over the final five years of the calibration planning horizon from 1998 to 2002, therefore the total number of decision variables is *N=215*. First the HG formulation in Equations 19a to 19c is developed and solved, then the CHT formulation in Equations 20a to 20f. A large portion of the computational effort during optimization is devoted to estimating the response matrix required in each nonlinear or outer iteration in which the linearized Lagrange subproblem is solved. When exclusively simulating the groundwater flow under the HG formulation nearly two minutes of runtime is required to simulate the five year management period; therefore simply estimating the response matrix requires at

least seven hours of runtime. Simulating coupled flow and transport roughly triples the simulation time and consequently triples the time to estimate the response matrix.

Table 5 presents the objective function values for the HG and CHT formulations after two nonlinear iterations along with the total recorded injected water over the same period. Only two nonlinear iterations are allowed in both formulations to maintain reasonable execution times but also to allow the convergence to be more closely monitored. For the HG and CHT formulations, two nonlinear iterations are respectively executed in approximately 28 and 143 hrs of runtime. The objective function values for the HG and CHT cases are consistent because in both cases a marginal change in the initial policy is realized yielding an objective function value that is slightly greater than the initial objective associated with the initial injection policy. The initial objective function value is $1.39*10^6$ ft^3/day ($3.95*10^4$ m^3/day) and the respective objective function values for the HG and CHT formulations are 1.5 and 3.3% higher, respectively as shown in Table 5. In both cases the simulation-optimization model could not improve upon the assigned initial policy.

Table 5: Objective Function Values for HG and CHT Formulations After Two Nonlinear Iterations with Total Recorded Injection from 1998 to 2002.

Scenario	**Objective (ft^3/day)**	**Nonlinear Iterations**	**Execution Time (hr)**
HG Formulation (*N=215, M=178)*	1,415,000	2	27.5
CHT Formulation (*N=215, M=356)*	1,436,000	2	143
Total Recorded Injection	845,000		

The optimized injection policies are examined more carefully to determine how the injection rates were altered during optimization. The change in the injection rate is plotted in Figure 13 for each of the 215 decision variables in both cases where the initial injection policy is subtracted from the optimized injection policy. Figure 13 shows that most decision variables are relatively unchanged yielding a value of 0. In the HG formulation only the values of six decision variables have been significantly reduced with three of these being driven to their lower bound while the values of 49 decision variables are increased during optimization, and 34 of these 49 are driven to their upper bound. For the HG formulation, the more extreme magnitude decrease in relatively fewer decision variables is offset by smaller, more frequent increases in a larger number of decision variables. The change in injection policy obtained when applying the CHT formulation is much more variable where 53 have been decreased relative to their initial value, 107 have been increased, and 55 remain unchanged. The net effect in both cases is a small increase in the objective function values when compared to their initial value.

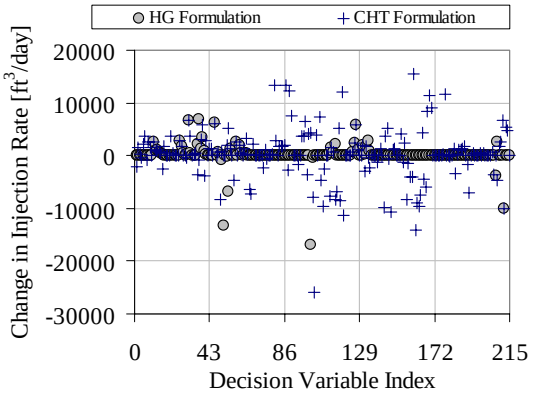

Figure 13: Injection Rate Difference for HG Formulation Transient Future Optimal Scheduling Problem.

A final optimization scenario is executed to verify that the simulation-optimization model performance will improve when the number of decision variables is reduced. This time a subset of three injection wells are considered in the optimization over the five year management period (1998-2002). The full HG formulation is adopted and a moderately conservative, and temporally non-uniform initial policy is assigned to each well prior to optimization. Table 6 shows the initial, optimized, and historical injection policies for the three wells considered: 492BC, 492BA, and 492BG.

Table 6: Injection Policies for Initial, Optimized, and Historical Operation for Wells 492BC 492BA, and 492BG.

Initial Policy (ft^3/day)						
Well ID	**Period 1**	**Period 2**	**Period 3**	**Period 4**	**Period 5**	**Sum**
492BC	4,000	4,500	5,000	5,500	6,000	25,000
492BA	3,000	1,000	2,000	5,000	6,048	17,048
492BG	2,000	3,000	3,500	3,000	3,996	15,496
					Total	57,544
Optimized Policy (ft^3/day)						
Well ID	**Period 1**	**Period 2**	**Period 3**	**Period 4**	**Period 5**	**Sum**
492BC	1,999	2,499	299	3,499	3,999	14,995
492BA	999	0	0	2,999	4,047	8,045
492BG	0	999	1,499	999	1,995	5,492
					Total	28,532
Historical Policy (ft^3/day)						
Well ID	**Period 1**	**Period 2**	**Period 3**	**Period 4**	**Period 5**	**Sum**
492BC	1,149	3,201	4,185	4,183	2,772	15,490
492BA	1,558	559	562	2,940	4,529	10,147
492BG	723	1,523	1,409	1,719	1,814	7,189
					Total	32,826

The optimization results in Table 6 are generally consistent with the two well test case and demonstrate that the simulation-optimization model performance is improved when considering a subset of the barrier injection wells. From Table 6 the initial objective function is $5.75*10^4$ ft^3/day ($1.63*10^3$ m^3/day) and converges to a value of $2.85*10^4$ ft^3/day ($8.08*10^2$ m^3/day) after three nonlinear iterations executing in about 9.5 hours. The corresponding historical injection is $3.28*10^4$ ft^3/day ($9.30*10^2$ m^3/day), 15% greater than the optimized injection rate. Notice also that the historical transient injection pattern of the wells is reproduced in the optimized solution.

Scenario 3 Results: Transient Optimal Scheduling Problem, Forward Operation

The third and final application of the OSP determines a future injection policy that will improve the barrier operation. For this scenario the HG formulation is adopted again containing 215 decision variables, the product of all 43 wells over a future five year planning horizon spanning 2003 to 2007. The head targets for the HG case are determined by taking predicted head at the beginning of 2003, and increasing the hydraulic head at the most sensitive targets by 5% with a base scenario equal to no improvement where head is maintained at 2003 levels. Initial simulation runs revealed

that the head could be feasibly increased by 5% at 90 of the 178 target sites shown in Figure 6, the remaining 88 targets are maintained at their 2003 base level. To begin optimization an initial policy is developed where for each well a significantly high injection rate approaching, but slightly less than, the maximum injection rate is uniformly assigned over the five year planning period. In this case selecting an initial policy that is feasible in meeting the proposed hydraulic constraints is critical; therefore a relatively high value of injection is prescribed at each well.

As before, the simulation-optimization model is limited to two nonlinear iterations in order that the objective function and convergence can be more closely monitored. Following the first two nonlinear iterations, the feasibility in the nonlinear hydraulic constraint set is verified, however only a slight reduction in the objective function could be achieved. The optimized policy output after two nonlinear iterations is then reassigned as the initial policy, and two additional nonlinear iterations are executed to determine if further improvement in the objective function could be realized.

Table 7 presents the initial objective function value, and the values after two and four nonlinear iterations as well as the execution time for both optimization runs. Notice the negligible 0.01% decrease in the objective function value following the first two nonlinear iterations, then another negligible increase in the objective function value is observed after the second set of iterations. These results are consistent with the previous transient injection scenario in which all 43 injection wells are included as decision variables and the efficiency of the simulation-optimization model is significantly reduced. Even though the simulation-optimization model is unable to improve upon the initial injection policy, the simulation-optimization results however suggest that assigning the prescribed initial policy will result in a quantifiable improvement in operation for the hydraulic barrier.

Table 7: Tracking Objective Function with Nonlinear Iterations for HG Formulation of Transient Optimal Scheduling Problem, Future Mode.

Injection Policy Description	Objective (ft^3/day)	Nonlinear Iterations	Runtime (hrs)
Initial	1,859,250	0	0
First Optimization Run	1,859,081	2	36
Second Optimization Run	1,859,162	4	31

Optimal Well Location Problem Scenario Results

The calibrated simulation model by itself is a valuable tool for evaluating parts of the injection barrier that can be improved without employing optimization. To briefly demonstrate, two simulations are conducted, in the first all injection wells are assigned their maximum rate, and in the second all injection wells are shut off over the calibration POR. The difference between head and concentration calculated by these two simulation runs are shown for the I Aquifer in Figure 14. In Figure 14a, three light colored areas along the alignment indicate areas of relatively low pressure head, and therefore carry an increased risk of future seawater intrusion. The difference in concentration in Figure 14b

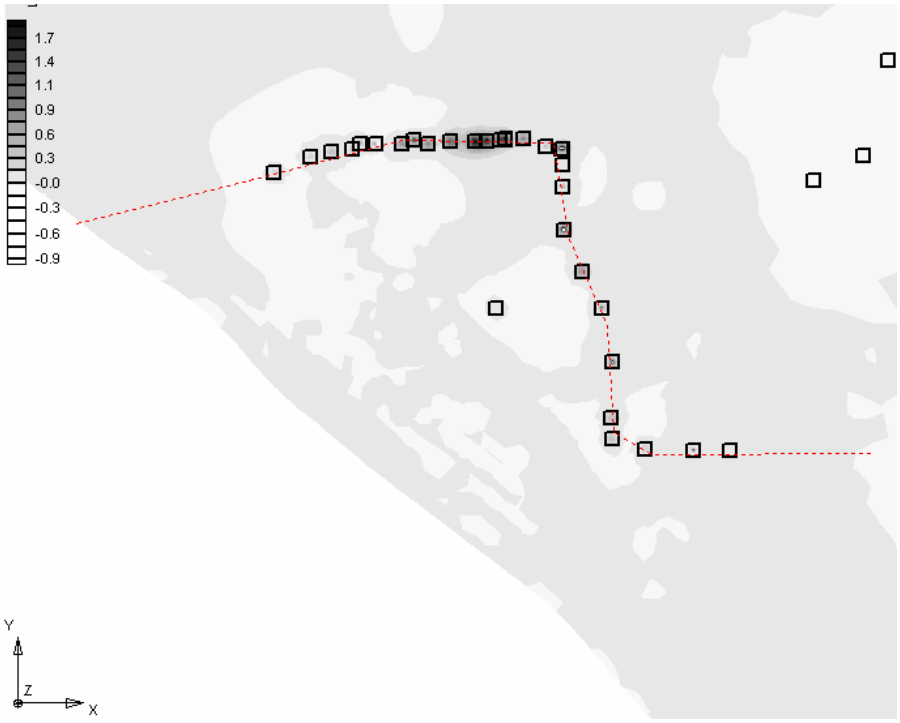

(a)

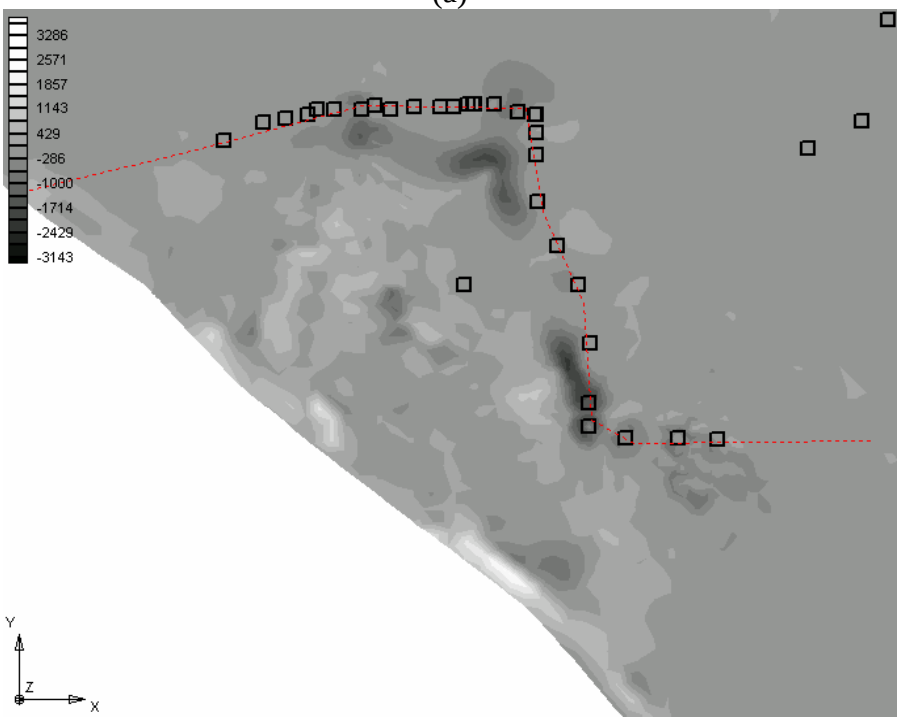

(b)

Figure 14: I Aquifer Sensitivity to State Variables, (a) Hydraulic Head (ft), (b) Chloride Concentration (ppm).

suggests that the upper left portion of the barrier has the greatest potential risk of rising chloride concentration. While simulations can provide insights as to regions of the barrier where the efficiency can be improved, optimal well locations are determined through simulation-optimization methods previously discussed. The OWLP algorithm in

Figure 5 is developed and executed on the UCLA Academic Technology Services Hoffman Cluster consisting of approximately 48 Intel Xenon dual processors.

The OWLP simulation-optimization model converged after about 10 hours of runtime on four processor nodes. Figure 15 shows the evolution of the fitness function over the course of generating 100 of populations, each containing four individuals. The maximum difference between the best and worst new well pairs is nearly 30 ft (9 m). The fitness initially trends in a steady positive direction for about the first five generations. The population is restarted for the first time after the twelfth generation, then the fitness tends to be much more random or scattered, although the fittest individual is repeatedly discovered with a fitness of 26.27 ft (8 m). After 56 generations a new optimum is discovered with a marginally improved fitness of 29.24 ft (8.91 m), which remains the fittest individual until the 75th generation in which the final fittest individual is discovered with a fitness equal to 29.36 ft (8.95 m). The top five individuals, their fitness, and the corresponding well node pairs are summarized in Table 5. Interesting is that all of the top ranked well pairs are located in the B aquifer. Furthermore, the new wells are clustered together near the existing injection well 503AY, working together with the existing well to cause the largest impact thereby maximizing the fitness function.

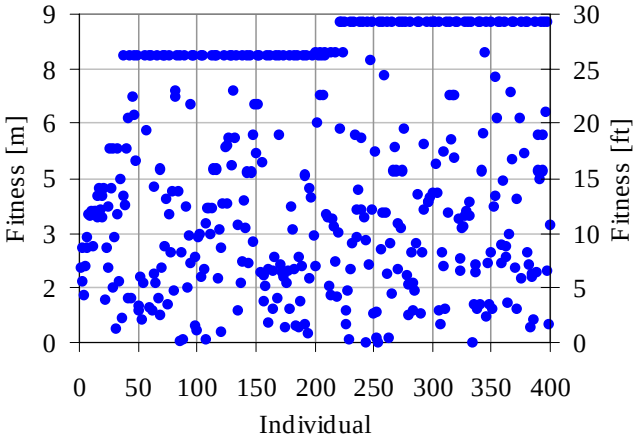

Figure 15: Evolution of Fitness for Each Individual Over Successive Generations.

Table 8: Top Five Optimized Well Pairs within 50 ft of Existing Barrier Alignment.

Rank	ID 1	ID 2	Well 1	Well 2	Fitness [ft]
1	883	875	(51961, 56961)	(51959, 56959)	29.36
2	883	879	(51961, 56961)	(51960, 56960)	29.24
3	883	871	(51961, 56961)	(51958, 56958)	26.46
4	849	875	(51952, 56952)	(51959, 56959)	26.45
5	883	868	(51961, 56961)	(51957, 56957)	26.27

CONCLUSIONS

Heterogeneous conductivity fields estimated by the NNK method are consistent in trend to previously published maps of local transmissivity at the study site in Callison *et al.* (1991). The NNK results show much more local variations. Small circular patterns evident in the field may be enhanced by the zonation schemes embedded in the NNK algorithm as the consequence of a set of highly variable prior estimates of hydraulic conductivity. The accuracy of the NNK method is based largely upon the prior parameter measurements. Therefore, the accuracy of the NNK results is highly dependent on both

the arrangement of the sample locations and the uncertainty associated with the estimates themselves.

A minimum LSE-CON is achieved when the longitudinal dispersivity is 15.2 m and the corresponding transverse dispersivity is 1.52 m. The rate of change in the overall model fit with a corresponding change in dispersivity, tends to decrease around the minimum LSE-CON. Also, the crossover effect is confirmed to be negligible in the transport calibration phase. In this case, a three order of magnitude increase in the transport parameters leads to a negligible increase of 0.3% in the LSE-HEAD. Additional adjustments to transport parameters for the most significant layers, the A and I aquifers, result in a negligible impact on the model error quantified as LSE-CON and LSE-HEAD.

Following the two-phase calibration, three alternative simulation-optimization models have been developed linking a calibrated simulation model with two optimization solvers. The first two optimization problems considered compare the simulation optimization results to the historical barrier operation while the latter two cases examine ways of improving the barrier's ability to mitigate future seawater intrusion. While some conclusions of this study are general and consistent with previous published studies, others are undoubtedly specific to the Alamitos Barrier Project.

A common trend has emerged when looking over all of the OSP scenarios considered; the efficiency of the gradient-based simulation-optimization model deteriorates as the number of decision variables increases. In the two well test case the simulation-optimization model identified a solution that met all constraints on hydraulic head and concentration by injecting 15% and 0.25% less water for wells 502M and 502P, respectively. In the three well test case, an injection policy is identified that injects 15% less water overall when compared to the corresponding historical record, while meeting all nonlinear targets on the hydraulic gradient. The steady injection OSP contained a moderate number of decision variables (*N=43*) and provided mixed results. When considering all 43 existing injection wells over a five year period the number of decision variables increases to *N=215* and the simulation-optimization model appears to have greater difficulty improving upon the initial policy.

Due to nonlinearity, interaction among the nonlinear decision variables becomes increasingly complex and non-intuitive. This is particularly evident in the case where many of the wells inject freshwater water into two, and in some cases up to four different aquifers, and therefore these wells are likely to be sensitive to a greater number of nonlinear target constraints. Also when both the hydraulic head and chloride concentration are considered in the formulation, the nonlinear relation between decision variables and constraints is enhanced.

When analyzing the operational flexibility of the system it is clear that the system is tight meaning that the feasible region for optimization is relatively small. A tight system reduces the efficiency of the optimization algorithm. Although only a small number of nonlinear iterations is allowed during execution of the simulation-optimization model, it is highly unlikely that further iterations will result in any significant improvements to the objective function.

When operated under the steady injection scenario, the simulation-optimization model tended to be conservative in that more water tended to be injected. The post optimization analysis of the two optimal steady-injection policies revealed a contrast in the two optimized solutions which essentially represent two different management strategies. The conservative IP-A results in an optimized policy in which more water is injected and a relatively higher factor of safety is attained in limiting seawater intrusion based on the greater frequency and uniform distribution of negative slacks in the transport targets referring back to Figure 11a and 11c. The other ambitious IP-B results in a policy which injects less water to maintain hydraulic targets, but also has a lower factor of safety in terms of meeting or maintaining concentration targets particularly in the deepest aquifers as evidenced by the positive trends in Figure 11b and 11d.

In the case of improving barrier operations, the simulation-optimization model is unable to improve upon an initial, feasible injection policy which would raise the hydraulic head by 5% at 90 of 178 targets. Future forward operations should focus on improving the hydraulic head in targeted regions along the barrier alignment, and include as decision variables only those wells that can influence the hydraulic gradient in these designated regions.

For the optimal well location problem, the fitness function, the marginal gain in head with newly added injection wells, rapidly increases in the first set of generations. A suboptimal individual of 26.27 ft (8 m) is identified after nine generations, then the maximum fitness function remains flat marginally increasing to slightly greater than 29 ft (8.8 m) after 56 generations. Furthermore, all of the top five fittest individuals are located in the B Aquifer referring back to Table 8. Also when adding two wells to the barrier alignment, the combinations resulting in the largest fitness function are those that are clustered together near an existing well and nearby observation target location where both new wells work together with the existing well to produce the greatest increase the head above the baseline value.

Finally, the success of the optimization formulations employed in this study for either the OSP or OWLP depend upon the target locations where state variables are monitored. Therefore sensitivity among these variable sets is important when selecting targets of which the formulations, and therefore results are based. The management application must guide the selection of target locations and the optimization formulation. If the process is conducted carefully and thoughtfully, then useful results will be efficiently achieved.

FINAL RECOMMENDATIONS

The simulation-optimization model linking MINOS with FEMWATER is clearly most efficient when the number of decision variables can be limited as in this case of optimizing a subset of the injection wells, for example. The OSP simulation-optimization model could be used on a real-time basis for operations and maintenance were a limited number of wells are optimized to determine the short term injection rates required to maintain hydraulic head targets while one well is shut off for maintenance. Also, the OWLP simulation-optimization model should be helpful in the future as one tool for quantifying and evaluating the benefit associated with candidate locations for new

injection wells. Simulations of the coupled flow and transport model can be used to identify regions of the barrier at highest risk of future seawater intrusion. Then the OWLP management model can then be used to identify the best locations for new wells within the region identified. The key to using the OWLP simulation-optimization model is a pre-optimization phase where the candidate locations for new wells are screened using well-defined management criteria.

The simulation-optimization models developed in this study are intended to be adapted and updated to improve accuracy as operational experience increases. Future research will focus on improving upon the optimal well location algorithm presented in Figure 5 including possible modifications to discourage clustering of new wells and alternative fitness formulations. Also the use of embedded optimization will be explored developing a hybrid GA similar to Tu *et al.* (2005) where both the location and injection rates of new injection wells are decision variables in a single, unified simulation-optimization model.

ACKNOWLEDGEMENTS

We would also like to thank Dr. Frank T-C. Tsai at LSU for his contributions to the calibration effort. We would also like to acknowledge the contributions and support of County of Los Angeles Department of Public Works and Academic Technology Services at UCLA. Thanks to our colleagues who have also helped edit previous drafts of this report.

REFERENCES

Banzhaf, W. P. Nordin, R. E. Keller, and F. D. Francone. 1998. Genetic Programming An Introduction. Morgan Kaufmann Publishers, Inc. San Francisco, CA. pps. 277-283.

Becker, L. and W. W-G. Yeh. 1972. Identification of Parameters in Unsteady Open Channel Flows. *Water Resources Research*, 8(4): 956-965.

Callison, J., M. Amabisco, A. Wilkins, and I. Nasseri. 1991. Hydrogeology of Alamitos Gap. Los Angeles County Department of Public Works, Hydraulic/Water Conservation Division Technical Report.

Carroll, D. L. 2004. "FORTRAN Genetic Algorithm (GA) Driver" *Available Online*: <http://cuaerospace.com/carroll/ga.html>. *Accessed on:* June 6, 2004.

Croucher, A. E., and M. J. O'Sullivan. 1995. The Henry problem for saltwater intrusion. *Water Resources Research* 31(7): 1809-1814.

Emch, P. G., W. W-G. Yeh. 1998. Management for Conjunctive Use of Coastal Surface Water and Groundwater. *Journal of Water Resources Planning and Management, ASCE*, 124(3): 129-139.

Essaid, H. L. 1990. A Multilayered Sharp Interface Model of Coupled Freshwater and Saltwater Flow in Coastal Systems: Model Development and Application. *Water Resources Research* 26(7): 1431-1454.

Finney, B. A., Samsuhadi, and R. Willis. 1992. Quasi-three-dimensional optimization model of Jakarta Basin. *Journal of Water Resources Planning and Management, ASCE*, 118(1): 18-31.

Frind, E. O. 1982. Simulation of long term density-dependent transport in ground water. *Advances in Water Resources* 5: 73-88.

Gelhar, L. W., C. Welty, and K. R. Rehfeldt. 1992. A Critical Review of Data on Field-Scale Dispersion in Aquifers. *Water Resources Research* 28(7): 1955-1974.

Gorelick, S. M., C. I. Voss, P. E. Gill, W. Murray, M. A. Saunders, and M. H. Wright. 1984. Aquifer reclamation design: The use of contaminant transport simulation combined with nonlinear programming. *Water Resources Research*, 20(4): 415-427.

Gorelick, S. M. 1983. A review of distributed parameter groundwater management modeling methods. *Water Resources Research*, 19(2): 305-319.

Gupta, N., and E. S. Bair. 1997. Variable-density flow in the midcontinent basins and arches region of the United States. *Water Resources Research*, 33(8): 1785-1802.

Harbaugh, A. W., and M. G. McDonald. 1996. User's documentation for MODFLOW-96; update to U.S. Geological Survey Modular Finite-Difference Ground-Water Flow Model. U.S. Geological Survey Open-File Report, 96-485. Reston, Va.

Henry, H. R. 1960. Salt intrusion into coastal aquifers. Ph.D. Dissertation, Department of Civil Engineering, Columbia University, New York, New York.

Journel, A. G., and C. Huijbregts. 1978. Mining geostatistics. Academic Press, London, United Kingdom.

Koch, M., and G. Zhang. 1993. Numerical simulation of the effects of variable density in a contaminant plume. *Ground Water* 30: 731-742.

Li, B. and T-C. J. Yeh. 1999. Cokriging Estimation of the Conductivity Field Under Variably Saturated Flow Conditions. *Water Resources Research* 35(12): 3663-3674.

Lin, H-C. J., D. R., Richards, C. A. Talbot, G-T. Yeh, J-R. Cheng, H-P. Cheng, and N. L. Jones. 1997. FEMWATER: A Three-Dimensional Finite Element Computer Model for Simulating Density-Dependent Flow and Transport in Variably Saturated Media. Technical Report CHL-97-12, US Army Engineer Research and Development Center, Waterways Experiment Station, Vicksburg, MS.

Louie, P., W. W-G. Yeh, and N. S. Hsu. 1984. Multiobjective water resources management planning. *Journal of Water Resources Planning and Management, ASCE*, 110(1): 39-56.

Murtagh, B. A., and M. A. Saunders. 1995. MINOS 5.4 User's Guide. Technical Report SOL 83-20R, Department of Operations Research, Stanford University, Stanford, Calif.

Olea, R. A. 1999. Geostatistics for Engineers and Earth Scientists. Kluwer Academic, Boston, Massachusetts.

RamaRao, B. S., A. M. La Venue, G. de Marsily, and M. G. Marietta. 1995. Pilot point methodology for automated calibration of an ensemble of conditionally simulated transmissivity fields 1. Theory and computational experiments. *Water Resources Research* 31(3): 475-493.

Reichard, E. G. and T. A. Johnson. 2005. Assessment of Regional Management Strategies for Controlling Seawater Intrusion. *Journal of Water Resources Planning. and Management*, 131(4): 280-291.

Royle, A., I. Clark, P. I. Brooker, H. Parker, A. Journel, J. M. Rendu, R. Sandefur, D. C. Grant, and P. F. Mousset-Jones. 1980. Geostatistics. McGraw-Hill Inc, New York, New York.

Schincariol, R. A., and F. W. Schwartz. 1990. An experimental investigation of variable density flow and mixing in homogeneous and heterogeneous media. *Water Resources Research* 26(10): 2317-2329.

Schrage, L. 1993. User's manual for linear, integer, and quadratic programming with LINDO, Release 5.3. Boyd and Fraser, Danvers, Mass.

Shamir, U., and G. Dagan. 1971. Motion of the seawater interface in coastal aquifers: A numerical solution. *Water Resources Research* 7(3): 644-657.

Shamir, U., J. Bear, and A. Gamliel. 1984. "Optimal annual operation of a coastal aquifer." *Water Resources Research*, 20(4): 435-444.

Sibson, R. 1981. "Chapter 2: A brief description of natural neighbour interpolation." In Interpreting Multivariate Data, Vic Barnett (Editor). John Wiley & Sons, New York, New York. pp 21-35.

Simmons, C. T. 2005. Variable density groundwater flow: From current challenges to future possibilities. *Hydrogeology Journal* 13: 116-119.

Simpson, M. J. and T. P. Clement. 2004. Improving the worthiness of the Henry problem as a benchmark for density-dependent groundwater flow models. *Water Resources Research* 40(1):10.1029/2003WR002199.

Tsai, F. T-C., and W. W-G. Yeh. 2004. Characterization and identification of aquifer heterogeneity with generalized parameterization and Bayesian estimation. *Water Resources Research* 40, (10):10.1029/2003WR002893.

Tsai, F. T-C., N-Z. Sun, and W. W-G. Yeh. 2005. Geophysical Parameterization and Parameterization Structure Identification Using Natural Neighbors in Groundwater Inverse Problems. *Journal of Hydrology,* 308: 269-283.

Tu, M-Y., F. T-C. Tsai, and W. W-G. Yeh. 2005. Optimization of Water distribution and Water Quality by Hybrid Denetic Algorithm. *Journal of Water Resources Planning and Management*, 131(6): 431-440.

Water Replenishment District of Southern California, 2004. Public Website. *Available Online*: <http://www.wrd.org/>. *Accessed on:* October 10, 2004.

Wilson, J., and A. Sa da Costa. 1982. Finite element simulation of a saltwater/freshwater interface with indirect toe tracking. *Water Resources Research* 18(4): 1069-1080.

Willis, R., and P. Liu. 1984. Optimization model for ground-water planning. *Journal of Water Resources Planning and Management, ASCE,* 110(3): 333-347.

Willis, R., and B. A. Finney. 1988. Planning model for optimal control of saltwater intrusion. *Journal of Water Resources Planning and Management, ASCE,* 114(2): 163-178.

Yeh, W. W-G. 1986. Review of parameter identification procedures in groundwater hydrology: The inverse problem. *Water Resources Research* 22(2): 95-108.